Federated Learning with NOMA Assisted by Multiple Intelligent Reflecting Surfaces

Latency Minimizing Optimization and Auction

Le, Tra Huong Thi; Cantos, Luiggi; Pandey, Shashi Raj; Shin, Hyundong; Kim, Yun Hee

Published in:
IEEE Transactions on Vehicular Technology

DOI (link to publication from Publisher):
10.1109/TVT.2023.3264202

Publication date:
2023

Document Version
Accepted author manuscript, peer reviewed version

Federated Learning with NOMA Assisted by Multiple Intelligent Reflecting Surfaces: Latency Minimizing Optimization and Auction

Tra Huong Thi Le, Luiggi Cantos, Shashi Raj Pandey, *Member, IEEE*, Hyundong Shin, *Fellow, IEEE*, and Yun Hee Kim, *Senior Member, IEEE*

***Abstract*—Federated learning (FL) has emerged as a promising framework to exploit massive data generated by edge devices in developing a common learning model while preserving the privacy of local data. In implementing FL over wireless networks, the participation of more devices is encouraged to alleviate the training inefficiency due to irregular local data but it tends to increase communication latency. To solve this problem, we address non-orthogonal multiple access (NOMA) assisted by intelligent reflecting surfaces (IRSs) to accommodate more devices and tailor their channels favorably to the FL performance. For the FL with IRS-NOMA, we minimize the total latency by reducing the latency per training round dominated by local computation and uplink communication through optimization of IRS-NOMA strategies and improving the training efficiency under irregular local data through active device selection. We then propose an auction-based IRS allocation that utilizes the optimized total latency for the valuation of the IRSs when multiple base stations of different operators share their neighboring IRSs. Winner determination (WD) and payment methods are devised with multiple bids on IRS subsets in a way of maximizing social welfare. The results show that the proposed latency minimizing algorithm outperforms the benchmarks by improving both communication and training efficiency through device selection combined with IRS-NOMA optimization. In addition, the auction mechanism with the proposed WD outperforms the benchmarks, where the social welfare is improved by constructing each bid with the valuation on multiple IRSs and increasing the number of bids submitted.**

***Index Terms*—Auction, federated learning, intelligent reflecting surfaces, non-orthogonal multiple access, device selection**

I. Introduction

Federated learning (FL) has attracted prodigious attention to exploit massive amounts of data generated by edge devices in developing various intelligent services [1]–[5]. Instead of sharing the data, the devices in FL share a common learning model with a model owner that is updated through local learning and model aggregation. As a result, FL ensures a certain level of privacy protection to local data at the devices while alleviating the communication burden of uploading large local data [4]. Therefore, FL, following its rise and maturation, is envisioned to become popular with wide applications not only in data-sensitive fields but also in distributive learning and optimization fields for future 6G networks [1], [3]–[5].

These emerging FL applications include small-scale FL scenarios where a single base station (BS) owns its learning model for the tasks related its serving area or devices such as edge computing and caching [2], dynamic traffic prediction for intelligent autonomous vehicles [5], and collaborative channel estimation [6] as well as large-scale FL scenarios where the devices and BSs distributed in a large area share a common learning model [7], [8]. When a delay-sensitive small-scale FL application is implemented over a resource-limited wireless network, the communication latency tends to come into prominence in the overall FL performance [9]–[13]. In particular, for FL under irregular local data distributions, it was observed that collaboration of more devices is necessary to build a reliable learning model faster [14]. However, initial studies on FL over wireless networks have resorted to orthogonal multiple access (OMA) schemes such as time division multiple access (TDMA), frequency division multiple access (FDMA), and orthogonal FDMA in aggregating the model parameters from multiple devices over a wireless network, which have shown the straggler effect dominated by a device suffering from a weak channel [9]–[13].

On the other hand, promising radio technologies have been suggested and investigated for 6G networks facing challenges of massive connectivity and resource scarcity [4], [15], [16]. Non-orthogonal multiple access (NOMA) has been identified as a viable multiple access candidate in supporting a large number of devices [17]–[19]. Therefore, NOMA can improve the convergence behavior of FL training under irregular local data by allowing more devices than OMA [9]–[13]. Intelligent reflecting surface (IRS), also known as reconfigurable intelligent surface (RIS), has emerged as a cost-effective performance booster that transforms propagation channels favorable to the desired performance by controlling reflecting components intelligently [15], [20], [21]. In particular when the direct channel from a device to a model owner suffers from blockages, an IRS can create a relay channel that enables participation of the device and reduces the straggler effect due to a weak channel observed in [9], [10].

Owing to the potential benefits of NOMA and IRS to FL, it is valuable and imperative to integrate them for FL to improve

T. H. T. Le, L. Cantos, H. Shin, and Y. H. Kim are with Department of Electronics and Information Convergence Engineering, Kyung Hee University, South Korea. E-mail: {huong_tra25, lrcantos, hshin, yheekim}@khu.ac.kr. S. R. Pandey is with the Connectivity Section, Department of Electronic Systems, Aalborg University, Denmark. Email: srp@es.aau.dk

This research was supported by the National Research Foundation of Korea (NRF) under Grant NRF-2021R1A2C1005869 and by the Institute of Information & Communications Technology Planning & Evaluation (IITP) under the Information Technology Research Center (ITRC) support program IITP-2023-2021-0-02046, with funding from the Ministry of Science and ICT (MSIT), Korea (*Corresponding author: Yun Hee Kim*).

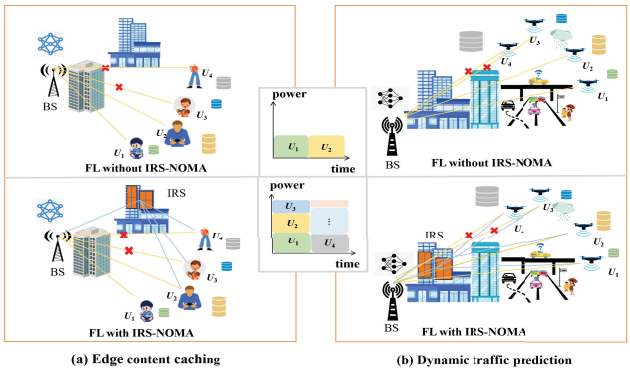

Fig. 1: Motivations of IRS-NOMA for emerging FL applications.

the communication efficiency and thereby to reduce the total training latency for emerging FL applications. Fig. 1 illustrates two examples of emerging delay-sensitive FL applications, edge computing and caching [2] and dynamic traffic prediction [5], which are implemented without and with IRS-NOMA. In [2], the popular contents related to a specific place for augmented reality (AR) were predicted and cached proactively through FL owned by the serving BS, where participation of more users in FL is encouraged to improve user experience by reducing the latency. In [5], dynamic traffic prediction with unmanned aerial vehicles (UAVs) was identified as a key application of FL, which requires a fast convergence of the training model through participation of more UAVs. However, the devices at users or UAVs that participate in FL can often suffer from blockages due to the obstacles such as high-rise buildings. With IRSs, more devices can communicate with the BS by creating the relay channels superseding the weak or unavailable direct channels. In the case, the BS, the model owner, can have more options to choose devices to cope with performance degradation caused by the heterogeneity of local data. Furthermore, NOMA allows more devices to upload their model in a given wireless resource, resulting in a faster convergence in FL training. In this way, a combination of IRS and NOMA reaps the benefits from both IRS and NOMA techniques in a way of reducing the training latency under a given performance requirement or improving the learning performance under a delay constraint.

In this regard, this paper considers a delay-sensitive small-scale FL built on an IRS-assisted NOMA network and optimizes the network to improve a convergence behavior of the FL training. Specifically, the IRS reflection, power allocation and decoding order of NOMA, and active devices participating in model aggregations are optimized to minimize the training latency under irregular local data distributions. Noticing that the FL performance of a BS can be improved by deploying more IRSs at appropriate locations, we subsequently propose a unique business model of an IRS provider that deploys IRSs in a communication region and rents the IRSs to their neighboring BSs to improve the performance of each BS's FL application. In a situation where the BSs compete one another in utilizing the IRSs, it is desirable for the BSs to estimate the values of the neighboring IRSs on their performance so that the IRS provider allocates the IRSs to the BSs based on their valuation of the IRSs. However, there are some challenges in allocating their IRSs to the BSs. Firstly, a BS may be self-interested without considering the utilities of the IRS provider and the other BSs. Secondly, a BS can cheat its valuation on a subset of IRSs to get a lower payment on using them. Thirdly, IRS allocation should be also beneficial to the BSs to encourage them to rent the IRSs with the payments. In this aspect, we address an IRS allocation problem to the designed FL system for which we design an auction process [22] to maximize a social welfare.

A. Related Works

1) IRS-assisted NOMA: IRS-assisted NOMA has been studied extensively for the downlink to optimize various performance metrics established for communication networks. Specifically, joint optimization of the IRS reflection and power allocation was studied without and with active beamforming to minimize the transmit power [23], [24], to optimize the sum rate [25], [26], to provide the physical layer security [27], and to maximize the minimum rate [28]. Multiple IRSs were also considered for the downlink NOMA in [29], where one IRS assists only one device for the NOMA signal constructed by two devices. The IRS-assisted uplink NOMA, which is required for model aggregation in FL, has not been studied as much as the downlink counterpart. Most studies on the IRS-assisted uplink NOMA have aimed at sum rate maximization [30]–[34] which optimizes IRS reflection only since the maximum sum rate is achieved with the maximum transmit power irrelevant of decoding order unless individual rate constraints are imposed. An efficient integration of IRS and NOMA for FL requires careful design considerations based on fairness rather than sum rate to guarantee a timely and successful transfer of the model parameters from each collaborating device. Although latency minimization problems were considered with IRS-assisted NOMA for mobile edge computing, they are formulated under different communication and computing scenarios by applying two-user NOMA for data offloading [35], [36].

2) FL with uplink NOMA: Uplink NOMA was considered for model aggregation in FL to improve the communication latency, where the gradient compression of the model parameters was uploaded to reduce the communication overhead [37]. Joint optimization of device scheduling and power allocation was studied to maximize the weighted sum rate of uplink NOMA for FL by taking into account the power capacity of devices [38]. The FL with uplink NOMA combined with wireless power transfer was proposed in [39], where the NOMA parameters, processing rates of the BS and devices, and accuracy of the FL training were optimized jointly to minimize a system cost in terms of the sum of energy consumption and FL convergence latency. However, the heterogeneity of local data was not considered in [39]. Our contribution lies in designing an IRS-assisted uplink NOMA to further improve the FL performance under the statistical heterogeneity in local data sets.

3) IRS-assisted FL: IRS-assisted FL was studied for over-the-air computation (AirComp) which aggregates the model parameters from multiple devices in signal waveforms by exploiting the superposition property of multiple access channels [40]–[45]. The mean square error (MSE) of the model parameters aggregated over the air is the major design criterion in these studies. The system parameters including IRS reflection were optimized to minimize the MSE jointly with device selection [40], [41] and maximize the number of participating devices under the MSE constraint [42]. In [43]–[45], AirComp for the model aggregation of FL was integrated with NOMA, where NOMA was used for separate data communication [43], [44] or for local model recovery by sending the symbols for AirComp redundantly. Although AirComp and NOMA have a similarity in power-domain sharing of wireless resources among the devices, their usages are different in the objectives and performance metrics. AirComp exhibits a lack of flexibility by transmitting symbol types appropriate for model aggregation over the air and hence requires a new air interface and signal processing at both the BS and devices dedicated to the FL operation. On the other hand, NOMA implementable on top of an existing air interface is flexible in accommodating diverse performance metrics and model aggregation methods including model compression [37].

4) Auction-Based Resource Allocation: Due to the efficiency in both process and outcome, auction is widely used for resource allocation in wireless networks. For instance, resource allocation among infrastructure providers, mobile virtual network operators, and devices was formulated as two-layer auction in [46]. Online auction based device-to-device offloading was proposed in [47] by taking into account the battery capacity of mobile devices. Randomized auction was also leveraged in spectrum sharing for co-located mobile edge computing [48]. To the best of the authors' knowledge, there exists no literature applying auction to the IRS allocation problem, where multiple BSs compete with one another to rent the IRSs installed by an IRS provider for the FL with IRS-assisted uplink NOMA.

B. Contributions

Although the uplink NOMA and IRSs were addressed to the FL individually, the synergy created by the two methods has been rarely explored from the viewpoint of the FL performance. In addition, multiple IRSs available in a region have not been considered as a resource to be rented to the BSs to improve their own FL tasks. In this regard, we consider a service region of an IRS provider where multiple BSs of different operators perform their own FL application through uplink NOMA by utilizing mutually exclusive subsets of the IRSs installed by the IRS provider. Each BS aims at minimizing the total latency of its own FL training to attain a certain test accuracy. To achieve the goal, two challenging problems should be addressed and tackled; i) How should each BS design the IRS-assisted NOMA to minimize the total latency of FL? ii) How should the IRS provider allocate the IRSs to the BSs when the BSs compete with each other? The first problem designed by addressing several FL features in optimizing IRS reflection, power allocation of NOMA, and device selection jointly is unique in the objective and constraints, and has not been tackled yet in the IRS-assisted NOMA literature. The second problem developed by a unique business model is solved via an auction-based IRS allocation mechanism to realize multiple FL tasks in a communication efficient fashion. The main contributions of this paper are summarized as follows:

- We first consider a small-scale FL scenario, where a BS develops its own FL model with its devices of different computing capabilities under irregular local data sets as in [14], [49] and aggregates local models through uplink NOMA assisted by a subset of multiple IRSs. In this setup, we formulate the problem of minimizing the total latency of the FL training subject to the individual rate constraints, where the total latency is modeled by the latency of one round of model aggregation and the number of rounds up to a convergence estimated through experiments taking into account local data distributions in a convergence behavior of the FL.
- For the first problem, we propose to solve the problem by minimizing the latency per round by optimizing IRS-NOMA parameters for a given set of active devices and searching for the best device set minimizing the total latency computed with the minimized latency per round. For IRS-NOMA optimization, we develop an alternating optimization (AO) algorithm optimizing power allocation of the devices and unit modulus reflection of the utilized IRSs alternately, where successive convex approximation (SCA) [50] is applied for power allocation problem and semidefinite relaxation (SDR) [51] is applied for IRS reflection optimization. For device selection, we propose a low-complexity algorithm based on the Markov chain approximation approach by designing an ergodic Markov chain and the transition probabilities that make the Markov chain converge to its stationary probabilities.
- Next, we consider an IRS allocation problem among nearby BSs of different operators in a way of minimizing the total latency of the FL task performed by each BS. For the problem, we propose an incentive auction between multiple BSs of different operators acting as bidders and an IRS provider acting as a seller and also as an auctioneer by adopting the inverse of the optimized total latency as a bidding value. Each BS assesses the values of the IRS subsets in improving its FL performance and submits multiple bids to the auctioneer. At the auctioneer, the winning IRS subsets are determined by adopting a greedy algorithm in order to maximize the social welfare. We also propose the payment scheme to achieve desirable auction properties such as truthfulness and individual rationality [22].

The rest of this paper is organized as follows. Section II describes the network architecture, FL model, and latency of FL training with IRS-assisted NOMA. We first formulate the total latency minimization problem for a single BS with a given subset of IRSs, followed by the algorithms solving the problem in Section III. An auction mechanism for IRS

allocation is presented in Section IV with the proofs of desirable auction properties. Numerical results for latency minimization and IRS allocation are then provided in Section V. Finally, conclusion is provided in Section VI.

Notation: Vectors and matrices are denoted by boldface lower-case and upper-case letters, respectively. The set of $n \times m$ matrices is denoted by $\mathbb{R}^{n\times m}$ for the real-valued entries and by $\mathbb{C}^{n\times m}$ for the complex-valued entries. The set of $n \times n$ semidefinite positive matrices is represented by $\mathbb{S}_+^n$. We use $\mathrm{diag}(\boldsymbol{a})$ to represent the diagonal matrix with a diagonal vector $\boldsymbol{a}$, $[\boldsymbol{a}]_n$ to denote the nth entry of a vector $\boldsymbol{a}$, and $[\boldsymbol{A}]_{n,m}$ to denote the (n, m)th entry of a matrix $\boldsymbol{A}$.

II. System Model

A. Network and Service Architecture

We consider a service region of an IRS provider, where the IRS provider installs multiple IRSs to assist to assist neighboring BSs in serving their intelligent devices. The BSs are owned by different operators and utilize distinct frequency bands licensed to their operators as in [52], [53]. Fig. 2(a) illustrates an example of a service region with four BSs and six IRSs. We denote the set of BSs by $\mathcal{M}$, the set of IRSs by $\mathcal{L}^{all}$, and the set of intelligent devices working for BS m by $\mathcal{K}_m^{all}$ for $m \in \mathcal{M}$. Each BS and each device are equipped with a single antenna whilst each IRS consists of N reflecting elements. The reflection vector of IRS l is denoted by

$$\boldsymbol{\phi}_l = [\phi_{l1}, \phi_{l2}, ..., \phi_{lN}]^T \in \mathbb{C}^{N\times 1} \tag{1}$$

consists of the complex numbers of unit modulus as $|\phi_{ln}| = 1$ for $l \in \mathcal{L}^{all}$ and $n \in \mathcal{N} \triangleq \{1, 2, \cdots, N\}$.

The deployed IRSs are the resources for the BSs to enhance their own FL applications as described in Fig. 2(b). An IRS can serve up to a single BS through reflection optimization but a BS can exploit multiple IRSs for its communication. Henceforth, the BSs compete with one another to obtain their favorable IRSs that improve the communication efficiency during their FL model training. We adopt an auction mechanism to establish such interactions between the BSs and IRS provider, which is performed in two stages. In the first stage, each BS valuates IRS subset candidates by estimating the minimum total latency achieved by IRS-assisted NOMA for each candidate in FL training, and submits the bids to the IRS provider. In the next stage, the IRS provider, based on the bids from the BSs, determines the winner BS for each IRS and informs the BSs to utilize their allocated IRSs.

B. FL model

We consider a small-scale FL where each BS owns its learning model specific to the task related to its service region or its devices in the region. The task is assumed to be delay-sensitive so that the model should be trained in a short time with the devices available in the region. Thus, we assume that the channel environment remains unchanged during the FL training process. Prior to starting an FL session, each BS m selects a set $\mathcal{K}_m \subset \mathcal{K}_m^{all}$ of devices participating in the FL session, which are referred to as active devices. Each device $k \in \mathcal{K}_m$ has a local data set $\mathcal{D}_{mk} = \{(\boldsymbol{x}_{mkd}, \boldsymbol{y}_{mkd})\}_{d=1}^{D_{mk}}$, where $\boldsymbol{x}_{mkd}$ and $\boldsymbol{y}_{mkd}$ are the d-th input and output of device k, respectively, and D_{mk} is the number of data samples in the local data set $\mathcal{D}_{mk}$.

The training process of an FL algorithm is performed in a way of solving the following optimization problem:

$$\min_{\boldsymbol{\omega}_m} F_m(\boldsymbol{\omega}_m) \tag{2}$$

where $\boldsymbol{\omega}_m$ is the global FL model generated by BS m and

$$F_m(\boldsymbol{\omega}_m) \triangleq \frac{1}{D_m} \sum_{k\in\mathcal{K}_m} \sum_{d=1}^{D_{mk}} f(\boldsymbol{\omega}_m, \boldsymbol{x}_{mkd}, \boldsymbol{y}_{mkd}) \tag{3}$$

is the global loss function computed with a loss function $f(\boldsymbol{\omega}_m, \boldsymbol{x}_{mkd}, \boldsymbol{y}_{mkd})$ and $D_m = \sum_{k\in\mathcal{K}_m} D_{mk}$. The loss function reflects the performance of the FL algorithm. During the FL session, each device $k \in \mathcal{K}_m$ updates its local model by minimizing

$$F_{mk}(\boldsymbol{\omega}_m) = \frac{1}{D_{mk}} \sum_{d=1}^{D_{mk}} f(\boldsymbol{\omega}_m, \boldsymbol{x}_{mkd}, \boldsymbol{y}_{mkd}) \tag{4}$$

whilst BS m updates the global model by aggregating the local updates as

$$F_m(\boldsymbol{\omega}_m) = \frac{1}{D_m} \sum_{k\in\mathcal{K}_m} D_{mk} F_{mk}(\boldsymbol{\omega}_m). \tag{5}$$

In this paper, each BS updates the model $\boldsymbol{\omega}_m$ for N_r training rounds[1], where each training round $t \in \{1, 2, \cdots, \mathsf{N}_r\}$ consists of the following procedure as in [54]:

i) Model broadcast: BS m broadcasts the current global model $\boldsymbol{\omega}_m^t$ to the active devices.

ii) Local model update: Each active device initializes its local model with the received global model as $\boldsymbol{\omega}_{mk,0}^t = \boldsymbol{\omega}_m^t$ and updates its local model with its local dataset $\mathcal{D}_{mk}$ as follows:

$$\boldsymbol{\omega}_{mk,j+1}^t = \boldsymbol{\omega}_{mk,j}^t - \eta \nabla F_{mk}|_{\boldsymbol{\omega}_m = \boldsymbol{\omega}_{mk,j}^t} \tag{6}$$

for $j = 0, 1, \cdots, \mathsf{l}_u - 1$, where l_u represents the number of local updates at the device assumed to be a fixed value, η is the learning rate, and ∇F_{mk} is the gradient of F_{mk} with respect to $\boldsymbol{\omega}_m$. The gradient is performed on the whole data set $\mathcal{D}_{mk}$ if we use gradient descent, and on the mini-batch $\mathcal{D}_{b,mk}$ of size d_{mk} sampled randomly from $\mathcal{D}_{mk}$ if we use the stochastic gradient [55].

iii) Local model upload: The active devices upload $\boldsymbol{\omega}_{mk}^t = \boldsymbol{\omega}_{mk,\mathsf{l}_u}^t$ to BS m.

iv) Model aggregation: The BS updates $\boldsymbol{\omega}_m^{t+1}$ with the received $\boldsymbol{\omega}_{mk}^t$ as

$$\boldsymbol{\omega}_m^{t+1} = \frac{\sum_{k\in\mathcal{K}_m} D_{mk} \boldsymbol{\omega}_{mk}^t}{\sum_{k\in\mathcal{K}_m} D_{mk}}. \tag{7}$$

[1]We use 'training round' and 'round' interchangeably in this paper, which correspond to one FL iteration consisting of model broadcast, local model update, local model upload, and model aggregation.

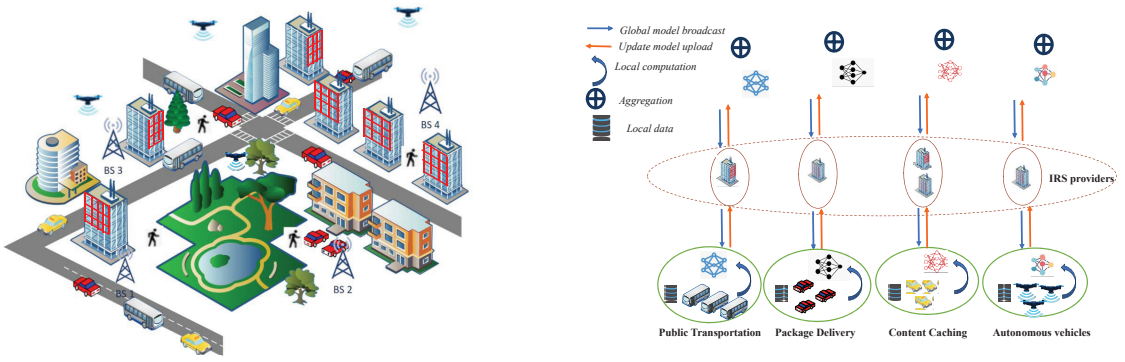

(a) (b)

Fig. 2: (a) System model with 4 BSs (b) FL processes with an IRS provider.

TABLE I: Table of notations

Notation	Description
$\mathcal{M}$; m	Set of BSs; BS index
$\mathcal{L}^{all}$; l	Set of IRSs; IRS index
N; n	Number elements of IRS l; element index
θ_{ln}; ϕ_{ln}	Phase shift of element n of IRS l; reflection of element n of IRS l
$\mathcal{K}_m^{all}$; $\mathcal{K}_m$	Set of total device of BS m; set of selected device of BS m
$\mathcal{D}_{mk}$; D_{mk}	Local dataset of device k of BS m; size of $\mathcal{D}_{mk}$
$\mathcal{D}_{bmk}$; d_{mk}	Mini-batch; mini-batch size of the local update of device k of BS m
$\mathcal{D}_m$; D_m	Global dataset of BS m; size of $\mathcal{D}_m$
F_{mk}; F_m	Local loss function of device of BS m; global loss function
$\boldsymbol{\omega}_{mk,j}^t$; $\boldsymbol{\omega}_m$	Local model of device k of BS m at round t; global weight of BS m
S_ω; N_r	Data size of local weight; number of training rounds
I_u; η	Number of local updates performed by the scheduled devices between two adjacent global aggregations; learning rate
p_{mk}; γ_{mk}	Transmit power of device; signal to interference and noise ratio of device $k \in \mathcal{K}_m$ at BS m at t-round
B_u; σ^2	Uplink bandwidth; noise power density
$\tilde{h}_{mk}$; $\boldsymbol{v}_{ml}$; $\boldsymbol{f}_{lk}$	Channel between BS and device; channel between BS and IRS; channel between BS and device
τ_{mk}^{cp}; τ_{mk}^{co}; $\Psi(\mathcal{K}_m)$	Computation latency per round; communication latency per round; latency per round
$\mathcal{C}_m^i$; b_m^i	Subset of IRSs chosen for the ith bid of BS m; bidding price of $\mathcal{C}_m^i$
J_m^i; q_m	Winner indicator of the ith bid of BS m; payment of BS m if BS m wins

C. Latency Model

This paper assumes that the latency of each training round consists of the device computation latency and uplink communication latency. The computation latency at the BS for the model aggregation is ignored due to the low complexity of the model aggregation and the relatively stronger computation capability of the BS. The downlink communication latency in model broadcasting is also ignored since the transmit power of the BS is much higher than the devices and the whole downlink bandwidth is dedicated to broadcasting the global model in general [55].

1) Device Computation Latency Model: We assume that the local processing rate of device $k \in \mathcal{K}_m$ is fixed during an FL session. The computation latency for the local model update in step ii) can be then obtained as

$$\tau_{mk}^{cp} = \frac{d_{mk}\mathsf{I}_u\nu}{\iota_{mk}}, \tag{8}$$

where d_{mk} is the minibatch size defined in step ii), ν is the required CPU cycle for processing each sample, and ι_{mk} is the local processing-rate in unit of CPU-cycle per second.

2) Communication Latency Model: We employ the uplink NOMA in step iii) so that the active devices upload their model $\boldsymbol{\omega}_{mk}^t$ of data size S_ω to BS m simultaneously. The communication latency incurred in step iii) is derived as follows.

Let the channels between BS m and device k, between BS m and IRS l, and between IRS l and device k denoted by $\tilde{h}_{mk} \in \mathbb{C}$, $\boldsymbol{v}_{ml} \in \mathbb{C}^{N\times 1}$, and $\boldsymbol{f}_{lk} \in \mathbb{C}^{N\times 1}$, respectively, which hold the channel reciprocity. The received signal at BS m can be expressed as

$$z_m = \sum_{k\in\mathcal{K}_m}\left(\tilde{h}_{mk} + \sum_{l\in\mathcal{L}_m}\boldsymbol{\rho}_{mkl}^T\boldsymbol{\phi}_l\right)s_k + \mathfrak{i}_m + \mathfrak{n}_m, \tag{9}$$

where $\boldsymbol{\rho}_{mkl} = \mathrm{diag}(\boldsymbol{v}_{ml})\boldsymbol{f}_{lk}$ is the relay channel from device k to BS m via IRS l, $\mathcal{L}_m$ is the IRS subset of BS m allocated through the auction process later, $\mathfrak{n}_m$ is the background noise with mean zero and variance σ^2, and

$$\mathfrak{i}_m = \sum_{l\in\mathcal{L}_m^c}\sum_{k\in\mathcal{K}_m}\boldsymbol{\rho}_{mkl}^T\boldsymbol{\phi}_l s_k \tag{10}$$

is the interference from the unallocated IRSs. Since the IRS reflection $\boldsymbol{\phi}_l$ is independent of $\boldsymbol{\rho}_{mkl}^T$ for the unallocated IRSs

$l \in \mathcal{L}_m^c$, $\mathfrak{i}_m$ can be modeled from the central limit theorem as complex Gaussian with mean zero and variance

$$\sigma_{\mathfrak{i}_m}^2 = \sum_{l \in \mathcal{L}_m^c} \sum_{k \in \mathcal{K}_m} \|\boldsymbol{\rho}_{mkl}\|^2. \tag{11}$$

We further define the multi-IRS reflection vector

$$\boldsymbol{\varphi}_m = [\boldsymbol{\phi}_{l_1}^T \ \boldsymbol{\phi}_{l_2}^T \ \cdots \ \boldsymbol{\phi}_{l_{|\mathcal{L}_m|}}^T]^T \tag{12}$$

and multi-IRS channel vector

$$\boldsymbol{h}_{mk} = [\boldsymbol{\rho}_{mkl_1}^T \ \boldsymbol{\rho}_{mkl_2}^T \ \cdots \ \boldsymbol{\rho}_{mkl_{|\mathcal{L}_m|}}^T]^T, \tag{13}$$

corresponding to the allocated IRSs, where $l_i \in \mathcal{L}_m$ and $l_i < l_{i+1}$. Then, (9) can be rewritten as

$$z_m = \sum_{k \in \mathcal{K}_m} (\tilde{h}_{mk} + \boldsymbol{\varphi}_m^T \boldsymbol{h}_{mk}) s_k + \mathfrak{i}_m + \mathfrak{n}_m. \tag{14}$$

The BS decodes each device's information from (14) through successive interference cancellation (SIC). We denote the decoding order as $\pi_m(k)$ for the device $k \in \mathcal{K}_m$, where $\pi_m(k) = n$ if the symbol of device k is decoded at the n-th order in SIC process; $\pi_m(k) < \pi_m(k')$ if device k is decoded earlier than device k' at BS m. With perfect SIC, we have

$$\gamma_{mk} = \frac{\left|\tilde{h}_{mk} + \boldsymbol{\varphi}_m^T \boldsymbol{h}_{mk}\right|^2 p_{mk}}{\sum\limits_{k' \in \mathcal{K}_m : \pi_m(k') > \pi_m(k)} \left|\tilde{h}_{mk'} + \boldsymbol{\varphi}_m^T \boldsymbol{h}_{mk'}\right|^2 p_{mk'} + \sigma_m^2}, \tag{15}$$

with $\sigma_m^2 = \sigma^2 + \sigma_{\mathfrak{i}_m}^2$, which leads to the achievable data rate of device $k \in \mathcal{K}_m$ with uplink bandwidth B_u as follows:

$$R_{mk} = B_u \log_2(1 + \gamma_{mk}). \tag{16}$$

Therefore, the uplink communication delay incurred by device $k \in \mathcal{K}_m$ in uploading the updated model to BS m is given by

$$\tau_{mk}^{co} = \frac{S_\omega}{R_{mk}}. \tag{17}$$

3) Total Latency in Training: We consider the synchronous model aggregation of FL so that the latency per training round is determined by the slowest device among the active devices in $\mathcal{K}_m$ as [55]

$$\Psi(\mathcal{K}_m) = \max_{k \in \mathcal{K}_m} (\tau_{mk}^{co} + \tau_{mk}^{cp}). \tag{18}$$

On the other hand, it was observed that the convergence rate increases linearly with the number of participating devices when local data sets $\{\mathcal{D}_{mk}\}_{k \in \mathcal{K}_m}$ are independent and identically distributed (iid) [14] while the rate increases nonlinearly when local data sets are non-iid [56]. From these observations, the number of rounds required to attain a certain test accuracy with an active device set $\mathcal{K}_m$ for the local data sets of a certain non-iid level can be approximated to [12]

$$\mathsf{N}_r(|\mathcal{K}_m|) = \left(\kappa + \frac{1}{|\mathcal{K}_m|}\right) G, \tag{19}$$

where G and κ depend on the non-iid level of local data sets and test accuracy as observed in the convergence analysis provided in Appendix. The parameters G and κ are estimated through the following experiments. Consider a group of devices with their local data sets exhibiting a certain non-iid level. The test accuracy in training a learning model with K participating devices is obtained as the number of training rounds increases with which the number $\mathsf{N}_r(K)$ of training rounds to meet the specified test accuracy is obtained. Performing this process with different K, we obtain multiple sample points of $(K, \mathsf{N}_r(K))$ with which the parameters G and κ are estimated through curve fitting.

The total latency of FL at BS m to obtain a desired accuracy is determined by multiplying the number of required training rounds (19) and the latency per training round (18) as

$$T_{total}(\mathcal{K}_m) = \Psi(\mathcal{K}_m) \left(\kappa + \frac{1}{|\mathcal{K}_m|}\right) G \tag{20}$$

when the channel is invariant over the training process. The total latency (20) exhibits a trade-off in computation-communication delay and training performance according to the number of participating devices. The number of training rounds required to achieve a given test accuracy is reduced by increasing the number of participating devices. However, more participating devices increase the latency per training round by increasing the communication latency in serving a more number of devices within a limited wireless resource. In addition, a BS can have a more chance to reduce the communication latency when more appropriate IRSs assist the uplink NOMA. In this regard, this paper optimizes the system resources available to each BS to minimize the total latency of its FL training.

III. Latency Minimizing Optimization

This section minimizes the total latency (20) of BS m in attaining a certain model accuracy of its FL training by assuming that an IRS subset $\mathcal{L}_m$ is allocated to the BS. This optimization process is required for valuation on the IRS subsets to design the IRS auction provided in the following section. This optimization process is similar for all BSs, we remove the BS index m in the following for the simplicity in notation.

The total latency minimization problem for a BS assisted by an IRS subset $\mathcal{L}$ is required to optimize the active device set $\mathcal{K}$, reflection vector of the IRS subset $\boldsymbol{\varphi}$, and NOMA parameters such as transmission power $\boldsymbol{p} = [p_{k_1}, p_{k_2}, \cdots, p_{k_{|\mathcal{K}|}}]^T$ of the active devices $k_i \in \mathcal{K}$ subject to $k_i < k_{i+1}$ and decoding order $\boldsymbol{\pi} = [\pi(k_1), \pi(k_2), \cdots, \pi(k_{|\mathcal{K}|})]^T$. In the optimization, we impose the individual rate constraints

$$R_k \geq R_{\min}, \ k \in \mathcal{K} \tag{21}$$

for the successful model uploading of the active devices. The total latency minimization problem jointly optimizing the IRS-NOMA parameters and active device set is then formulated as

$$\textbf{BS-IRS}: \quad \min_{\mathcal{K}, \boldsymbol{\varphi}, \boldsymbol{p}, \boldsymbol{\pi}, \Psi} \Psi \left(\kappa + \frac{1}{|\mathcal{K}|}\right) G \tag{22}$$

$$\text{s.t.} \quad \Psi \geq \tau_k^{co} + \tau_k^{cp}, \ k \in \mathcal{K}, \tag{22a}$$

$$R_k \geq R_{\min}, \ k \in \mathcal{K}, \tag{22b}$$

$$0 < p_k \leq p_k^{\max}, \ k \in \mathcal{K}, \tag{22c}$$

$$|\phi_{ln}| = 1,\ n \in \mathcal{N},\ l \in \mathcal{L}, \tag{22d}$$
$$\boldsymbol{\pi} \in \Pi, \tag{22e}$$
$$\mathcal{K} \subset \mathcal{K}^{all}, \tag{22f}$$

where Π is the set of all possible decoding orders and $\mathcal{K}^{all}$ is the set of all possible devices working for the BS.

The problem **BS-IRS** is challenging due to the constraints entangled with the active device set $\mathcal{K}$ in particular. Thus, we reformulate the problem **BS-IRS** in an equivalent form of two nested problems, searching for the best active device set after minimizing the latency-per-round for each active device set candidate as follows:

$$\text{(PD)}: \quad \min_{\mathcal{K}} \quad \Psi^\star(\mathcal{K}) \left(\kappa + \frac{1}{|\mathcal{K}|}\right) G \tag{23a}$$
$$\text{s.t.} \quad \text{(22f)}, \tag{23b}$$

where $\Psi^\star(\mathcal{K})$ is the optimized value of the latency-per-round minimization problem for given $\mathcal{K}$ as

$$\text{(PI)}: \quad \min_{\boldsymbol{\varphi},\boldsymbol{p},\boldsymbol{\pi},\Psi} \quad \Psi \tag{24}$$
$$\text{s.t.} \quad \text{(22a)} - \text{(22e)}. \tag{24a}$$

The solution of **BS-IRS** is given by $\{\boldsymbol{\varphi}^\star(\mathcal{K}^\star), \boldsymbol{p}^\star(\mathcal{K}^\star), \boldsymbol{\pi}^\star(\mathcal{K}^\star), \Psi^\star(\mathcal{K}^\star)\}$, where $\{\boldsymbol{\varphi}^\star(\mathcal{K}), \boldsymbol{p}^\star(\mathcal{K}), \boldsymbol{\pi}^\star(\mathcal{K}), \Psi^*(\mathcal{K})\}$ denotes the solution of (24) and $\mathcal{K}^\star$ denotes the final solution of (23).

Next, we first propose an algorithm to solve problem (PI) and then an algorithm for (PD) using the algorithm for (PI).

A. Latency-Per-Round Optimization

This subsection tackles problem (PI) for a given active device set $\mathcal{K}$ by optimizing power allocation $\boldsymbol{p}$ and IRS reflection $\boldsymbol{\theta}$ while employing a suboptimal decoding order $\boldsymbol{\pi}$ due to the formidable complexity in finding the optimal decoding order obtained after optimizing $\boldsymbol{p}$ and $\boldsymbol{\theta}$ for each of $|\mathcal{K}|!$ possible decoding orders. This paper considers up to I_{ord} different decoding orders $\boldsymbol{\pi}_l, l = 1, 2, \cdots$, where the initial decoding order $\boldsymbol{\pi}_0$ is obtained in descending order of the maximally achievable channel power of each device when the IRS reflection is optimized for that device as [28], [30]

$$\max_{\boldsymbol{\varphi}} \ p_k^{\max} |\tilde{h}_k + \boldsymbol{\varphi}^T \boldsymbol{h}_k|^2 \quad \text{s.t.} \quad \text{(22d)}. \tag{25}$$

The optimal value of (25) is given by $\chi_k^{\max} = p_k^{\max} |\tilde{h}_k + \sum_{n=1}^{N|\mathcal{L}|} |[\boldsymbol{h}_k]_n||^2$ with $[\boldsymbol{\varphi}]_n = e^{j(\angle \tilde{h}_k - \angle [\boldsymbol{h}_k]_n)}$ for $n = 1, 2 \cdots, N|\mathcal{L}|$ so that $\pi(k) \leq \pi(k')$ if $\chi_k^{\max} \geq \chi_{k'}^{\max}$. The decoding order $\boldsymbol{\phi}_l$ for $l > 0$ will be delineated later. For the given decoding order $\boldsymbol{\pi}_l$, we solve problem (PI) through alternating optimization (AO) of power allocation and IRS reflection as follows.

1) Transmit Power Optimization: For given IRS reflection $\boldsymbol{\varphi}$ and decoding order $\boldsymbol{\pi}$, (PI) is reduced to

$$\text{(PI1)}: \quad \min_{\boldsymbol{p},\Psi>0} \quad \Psi \tag{26}$$
$$\text{s.t.} \quad \frac{S_\omega}{B_u(\Psi - \tau_k^{cp})} \leq \log_2(1+\gamma_k),\ k \in \mathcal{K}, \tag{26a}$$
$$\frac{R_{\min}}{B_u} \leq \log_2(1+\gamma_k),\ k \in \mathcal{K}, \tag{26b}$$
$$0 \leq p_k \leq p_k^{\max},\ k \in \mathcal{K} \tag{26c}$$

Algorithm 1 SCA algorithm for power allocation

1: **Input:** IRS reflection $\boldsymbol{\varphi}$
2: Initialize $\boldsymbol{p}_s^{(0)}$and $\Psi_s^{(0)}$. Set $i = 0$.
3: **repeat**
4: $\quad i \leftarrow i + 1$.
5: $\quad$ Obtain $\Psi_s^{(i)}$ and $\boldsymbol{p}_s^{(i)}$ by solving problem (P11b).
6: **until** $(|\Psi_s^{(i)} - \Psi_s^{(i-1)}| <= \epsilon\ )$ or $(i \geq I_{sca})$
7: **Output:** $\boldsymbol{p}^o = \boldsymbol{p}_s^{(i)}$ and $\Psi^o = \Psi_s^{(i)}$

by using $\tau_k^{co} = S_\omega / R_k$ and $R_k = B_u \log_2(1+\gamma_k)$. We further express

$$\log_2(1+\gamma_k) = \Omega_k(\boldsymbol{p}) - \Theta_k(\boldsymbol{p}), \tag{27}$$

where $\Omega_k(\boldsymbol{p}) = \log_2(\sum_{\pi(k') \geq \pi(k)} X_{k'} p_{k'} + \sigma^2)$ and $\Theta_k(\boldsymbol{p}) = \log_2(\sum_{\pi(k') > \pi(k)} X_{k'} p_{k'} + \sigma^2)$ with $X_k = |\tilde{h}_k + \boldsymbol{\varphi}^T \boldsymbol{h}_k|^2$. Thus, problem (PI1) is rewritten as

$$\text{(PI1a)}: \quad \min_{\boldsymbol{p},\Psi>0} \quad \Psi \tag{26}$$
$$\text{s.t.} \quad \frac{S_\omega}{B_u(\Psi - \tau_k^{cp})} \leq \Omega_k(\boldsymbol{p}) - \Theta_k(\boldsymbol{p}),\ k \in \mathcal{K}, \tag{28a}$$
$$\frac{R_{\min}}{B_u} \leq \Omega_k(\boldsymbol{p}) - \Theta_k(\boldsymbol{p}),\ k \in \mathcal{K}, \tag{28b}$$
$$0 \leq p_k \leq p_k^{\max},\ k \in \mathcal{K}, \tag{28c}$$

which is a difference of convex functions (DC) programming known to be nonconvex. To find a local optimal solution, we apply the successive convex approximation (SCA) algorithm as

$$\text{(PI1b)}: \quad \min_{\boldsymbol{p}\geq 0, \Psi_s > 0} \quad \Psi \tag{29}$$
$$\text{s.t.} \quad \frac{S_\omega}{B_u(\Psi - \tau_k^{cp})} - \Omega_k(\boldsymbol{p}) + \tilde{\Theta}_k(\boldsymbol{p}, \boldsymbol{p}_s^{(i-1)}) \leq 0, k \in \mathcal{K}, \tag{29a}$$
$$\frac{R_{\min}}{B_u} - \Omega_k(\boldsymbol{p}) + \tilde{\Theta}_k(\boldsymbol{p}, \boldsymbol{p}^{(i-1)}) \leq 0,\ k \in \mathcal{K}, \tag{29b}$$
$$0 \leq p_k \leq p_k^{\max},\ k \in \mathcal{K}, \tag{29c}$$

where

$$\tilde{\Theta}_k(\boldsymbol{p}, \boldsymbol{p}_s) = \Theta_k(\boldsymbol{p})_s + \nabla \Theta_k(\boldsymbol{p}_s)(\boldsymbol{p} - \boldsymbol{p}_s) \tag{30}$$

is the first-order Taylor series approximation of $\Theta_k(\boldsymbol{p})$ at $\boldsymbol{p} = \boldsymbol{p}_s$ and $\boldsymbol{p}_s^{(i-1)}$ is the solution obtained at the previous iteration. Since the left-hand-sides of (29a) and (29b) become convex, problem (PI1a) is a convex problem so that we can solve the problem by using an existing convex optimization solver like CVX [57]. The SCA algorithm for power allocation is summarized in Algorithm 1 with a tolerance ϵ and maximum number I_{sca} of SCA iterations.

2) IRS Reflection Optimization: For given transmission power $\boldsymbol{p}$ and decoding order $\boldsymbol{\pi}$, problem (PI) becomes

$$\text{(PI2)}: \min_{\boldsymbol{\varphi},\Psi>0} \quad \Psi \tag{31}$$

$$\text{s.t.} \quad \frac{S_\omega}{B_u(\Psi-\tau_k^{cp})} \le \log_2(1+\gamma_k),\ k\in\mathcal{K}, \tag{31a}$$

$$\frac{R_{\min}}{B_u} \le \log_2(1+\gamma_k),\ k\in\mathcal{K}, \tag{31b}$$

$$|\phi_{ln}|=1,\ l\in\mathcal{L},\ n\in\mathcal{N}, \tag{31c}$$

which can be transformed as follows:

$$\text{(PI2a)}: \min_{\boldsymbol{\varphi},\Psi>0} \quad \Psi \tag{31}$$

$$\text{s.t.} \quad u_k(\Psi)\le\gamma_k(\boldsymbol{\varphi}),\ k\in\mathcal{K}, \tag{32a}$$

$$|\phi_{ln}|=1,\ l\in\mathcal{L},\ n\in\mathcal{N}, \tag{32b}$$

where

$$u_k(\Psi)=\max(2^{\frac{R_{\min}}{B_u}}-1, 2^{\frac{S_\omega}{B_u(\Psi-\tau_k^{cp})}}-1) \tag{33}$$

and

$$\gamma_k(\boldsymbol{\varphi})=\frac{|\boldsymbol{h}_k^T\boldsymbol{\varphi}+\tilde{h}_k|^2p_k}{\sum_{\pi(k')>\pi(k)}|\boldsymbol{h}_{k'}^T\boldsymbol{\varphi}+\tilde{h}_{k'}|^2p_{k'}+\sigma^2}. \tag{34}$$

By defining $\tilde{\boldsymbol{\varphi}}=[\boldsymbol{\varphi}^T\ 1]^T$ and $\boldsymbol{S}=\tilde{\boldsymbol{\varphi}}\tilde{\boldsymbol{\varphi}}^H\in\mathbb{S}_+^{N|\mathcal{L}|+1}$, we have

$$|\boldsymbol{h}_k^T\boldsymbol{\varphi}+\tilde{h}_k|^2=\tilde{\boldsymbol{\varphi}}^H\boldsymbol{C}_k\tilde{\boldsymbol{\varphi}}=\text{tr}(\boldsymbol{C}_k\boldsymbol{S}) \tag{35}$$

with

$$\boldsymbol{C}_k=\begin{bmatrix}\boldsymbol{h}_k^*\boldsymbol{h}_k & \boldsymbol{h}_k^*\tilde{h}_k\\ \tilde{h}_k^*\boldsymbol{h}_k^T & |\tilde{h}_k|^2\end{bmatrix}. \tag{36}$$

Problem (PI2) is then reformulated with $\boldsymbol{S}$ after relaxing the rank-one constraint, i.e., rank$(\boldsymbol{S})=1$, as

$$\min_{\boldsymbol{S}\in\mathbb{S}_+^{N|\mathcal{L}|+1},\Psi>0} \quad \Psi \tag{37}$$

$$\text{s.t.} \quad u_k(\Psi)\Big(\sum_{\pi(k')>\pi(k)}\text{tr}(\boldsymbol{C}_{k'}\boldsymbol{S})p_{k'}+\sigma^2\Big)\le\text{tr}(\boldsymbol{C}_k\boldsymbol{S})p_k, \tag{37a}$$

$$[\boldsymbol{S}]_{n,n}=1,\ n=1,2,\cdots,N|\mathcal{L}|+1, \tag{37b}$$

which is still non-convex due to constraint (37a). To handle this problem, we decouple $\boldsymbol{S}$ and Ψ by employing the bisection search method to find the maximum Ψ providing the feasible solution of $\boldsymbol{S}$. Specifically, for $\Psi_{\min}=\max_{k\in\mathcal{K}}\tau_k^{cp}$ and $\Psi_{\max}$ is given by the optimal value Ψ^o obtained in Algorithm 1, we initialize $\bar{\Psi}=\frac{\Psi_{\min}+\Psi_{\max}}{2}$. We then solve the feasibility problem given by

$$\text{(PI2b)} \quad \text{find} \quad \boldsymbol{S}\in\mathbb{S}_+^{N|\mathcal{L}|+1} \tag{38a}$$

$$\text{s.t.} \quad u_k(\bar{\Psi})\sum_{\pi(k')>\pi(k)}\text{tr}(\boldsymbol{C}_{k'}\boldsymbol{S})p_{k'}+u_k(\bar{\Psi})\sigma^2$$

$$\le\text{tr}(\boldsymbol{C}_k\boldsymbol{S})p_k,\ k\in\mathcal{K}, \tag{38b}$$

$$[\boldsymbol{S}]_{n,n}=1,\ n=1,2,\cdots,N|\mathcal{L}|+1, \tag{38c}$$

of which the feasible solution is denoted by $\boldsymbol{S}_{\bar{\Psi}}$. While updating $\bar{\Psi}$ through the bisection search method, we solve (PI2b) until we find the maximum $\Psi^\dagger$ that produces the feasible solution $\boldsymbol{S}^\dagger=\boldsymbol{S}_{\bar{\Psi}^\dagger}$. If the solution $\boldsymbol{S}^\dagger$ is not rank-one, we apply the Gaussian randomization process to obtain a rank-one solution from $\boldsymbol{S}^\dagger$ as in [28]. The process generates C random samples as

$$\tilde{\boldsymbol{\varphi}}^{(c)}\sim\mathcal{CN}(\boldsymbol{0},\boldsymbol{S}^\dagger),\ i=1,2,\cdots,C \tag{39}$$

to obtain feasible rank-one candidates as [28], [58]

$$\boldsymbol{\varphi}^{(c)}=\{e^{j\angle[\tilde{\boldsymbol{\varphi}}^{(c)}]_n-\angle[\tilde{\boldsymbol{\varphi}}^{(c)}]_{N|\mathcal{L}|+1}}, n=1,2,\cdots,N|\mathcal{L}|\}. \tag{40}$$

Among the rank-one candidates, we find the best candidate minimizing Ψ in (PI2a). The overall IRS reflection optimization process is summarized in Algorithm 2 which outputs the optimized IRS reflection vector $\boldsymbol{\varphi}^\dagger$.

Algorithm 2 SDR-based algorithm for IRS reflection optimization.

1: **Input:** transmission power $\boldsymbol{p}$
2: Initialize $\Psi_{\min}$ and $\Psi_{\max}$.
3: **while** $\Psi_{\max}-\Psi_{\min}\ge\epsilon$ **do**
4: Solve problem (P12b) with $\bar{\Psi}=\frac{\Psi_{\min}+\Psi_{\max}}{2}$.
5: **if** problem (P12b) is feasible **then**
6: $\boldsymbol{S}^\dagger\leftarrow\boldsymbol{S}_{\bar{\Psi}}$.
7: $\Psi_{\max}\leftarrow\bar{\Psi}$.
8: **else**
9: $\Psi_{\min}\leftarrow\bar{\Psi}$.
10: **end if**
11: **end while**
12: **for** $c=1,2,\cdots,C$ **do**
13: Generate a Gaussian random vector $\tilde{\boldsymbol{\varphi}}^{(c)}\sim\mathcal{CN}(\boldsymbol{0},\boldsymbol{S}^\dagger)$.
14: Obtain a candidate solution $\boldsymbol{\varphi}^{(c)}=\{e^{j\angle[\tilde{\boldsymbol{\varphi}}^{(c)}]_n-\angle[\tilde{\boldsymbol{\varphi}}^{(c)}]_{N|\mathcal{L}|+1}}, n=1,2,\cdots,N|\mathcal{L}|\}$
15: Obtain the objective value $\Psi^{(c)}$ of (P12a) with $\boldsymbol{\varphi}=\boldsymbol{\varphi}^{(c)}$.
16: **end for**
17: Find the best candidate $c^\dagger=\arg\max_{1\le c\le C}\Psi^{(c)}$.
18: **Output:** $\boldsymbol{\varphi}^\dagger=\boldsymbol{\varphi}^{(c^\dagger)}$

3) Overall Algorithm: The overall algorithm to solve latency-per-round minimization problem (PI) is summarized in Algorithm 3. For the given decoding order $\boldsymbol{\pi}_l$, AO of power allocation and IRS reflection (from line 4 to line 9) is performed until the objective value $\Psi_l^{(i)}$ is converged or the maximum number I_{AO} of AO iterations is reached, where $\Psi(\boldsymbol{p},\boldsymbol{\varphi},\boldsymbol{\pi})$ denotes the objective value computed with $(\boldsymbol{p},\boldsymbol{\varphi},\boldsymbol{\pi})$. With the optimized $\boldsymbol{p}_l^\star$ and $\boldsymbol{\varphi}_l^\star$ of the AO algorithm, we validate the decoding order by computing the power of each device's reconfigured channel as

$$\chi_k(\boldsymbol{p}_l^\star,\boldsymbol{\varphi}_l^\star)=[\boldsymbol{p}_l^\star]_k|\tilde{h}_k+\boldsymbol{h}_k^T\boldsymbol{\varphi}_l^\star|^2 \tag{41}$$

and updating the decoding order $\boldsymbol{\pi}_{l+1}$ in descending order of (41). The algorithm stops if either the decoding order $\boldsymbol{\pi}_{l+1}$ after optimization is not changed form $\boldsymbol{\pi}_l$ before optimization or the maximum number I_{ord} of decoding order updates is reached. The final solution is given by the best outcome among the decoding order candidates with which the AO of $\boldsymbol{p}$ and $\boldsymbol{\varphi}$ is performed.

Algorithm 3 Algorithm for latency-per-round minimization.

1: **Input:** active device set $\mathcal{K}$
2: Initialize $\boldsymbol{\pi}_0$ in descending order of $\chi_k^{\max}$, $\Psi_0^\star = \infty$, and $l = 0$.
3: **repeat**
4: Initialize $\boldsymbol{p}^{(0)} = \boldsymbol{p}^{\max}$, $\boldsymbol{\varphi}^{(0)}$ with $\theta_{ln} \sim \mathrm{U}(0, 2\pi)$, and and set iteration index $i = 0$.
5: **repeat**
6: $i \leftarrow i + 1$.
7: *Transmit power allocation*: Given $\boldsymbol{\varphi}^{(i-1)}$ and $\boldsymbol{\pi}_l$, solve problem (P11) via **Algorithm 1** with $\boldsymbol{p}_s^{(0)} = \boldsymbol{p}^{(i-1)}$ to obtain Ψ^o and $\boldsymbol{p}^{(i)} = \boldsymbol{p}^o$.
8: *IRS reflection optimization*: Given $\boldsymbol{p}^{(i)}$ and $\boldsymbol{\pi}_l$, solve problem (P12) via **Algorithm 2** with $\Psi_{\max} = \Psi^o$ to obtain $\boldsymbol{\varphi}^{(i)} = \boldsymbol{\varphi}^\dagger$.
9: Compute $\Psi_l^{(i)} = \Psi(\boldsymbol{p}^{(i)}, \boldsymbol{\varphi}^{(i)}, \boldsymbol{\pi}_l)$.
10: **until** $(|\Psi_l^{(i)} - \Psi_l^{(i-1)}| \leq \epsilon)$ or $(i \geq I_{AO})$
11: $l \leftarrow l + 1$.
12: Update $\Psi_l^\star = \Psi^{(i)}$, $\boldsymbol{p}_l^\star = \boldsymbol{p}^{(i)}$, and $\boldsymbol{\varphi}_l^\star = \boldsymbol{\varphi}^{(i)}$.
13: Update $\boldsymbol{\pi}_l$ in descending order of $\chi_k(\boldsymbol{p}_l^\star, \boldsymbol{\varphi}_l^\star)$.
14: **until** $(\boldsymbol{\pi}_l = \boldsymbol{\pi}_{l-1})$ or $(l \geq I_{ord})$
15: Find $l^\star = \arg\min_l \Psi_l^\star$.
16: **Output:** $\Psi^\star = \Psi_{l^\star}^\star$, $\boldsymbol{p}^\star = \boldsymbol{p}_{l^\star}^\star$, $\boldsymbol{\varphi}_{l^\star}^\star = \boldsymbol{\varphi}_{l^\star}^\star$, $\boldsymbol{\pi}^\star = \boldsymbol{\pi}_{l^\star}$.

For given decoding order $\boldsymbol{\pi}_l$, the AO iteration (from line 4 to line 9) in Algorithm 3 produces the objective value $\Psi_l^{(i)} = \Psi(\boldsymbol{p}^{(i)}, \boldsymbol{\varphi}^{(i)}, \boldsymbol{\pi}_l)$ that satisfies $\Psi_l^{(i)} \leq \Psi_l^{(i+1)}$ from

$$\begin{aligned}\Psi(\boldsymbol{p}^{(i)}, \boldsymbol{\varphi}^{(i)}, \boldsymbol{\pi}_l) &\geq \Psi(\boldsymbol{p}^{(i+1)}, \boldsymbol{\varphi}^{(i)}, \boldsymbol{\pi}_l) \\ &\geq \Psi(\boldsymbol{p}^{(i+1)}, \boldsymbol{\varphi}^{(i+1)}, \boldsymbol{\pi}_l).\end{aligned} \tag{42}$$

The first inequality results from Algorithm 1 and the second inequality results from Algorithm 2. Thus, the AO algorithm for the given decoding order $\boldsymbol{\pi}_l$ guarantees a convergence to a locally optimal solution. The overall algorithm selecting the best outcome among those achieved with different decoding orders also provides a locally optimal solution.

B. Active Device Selection

This subsection solves the active device selection problem (PD) through the Markov approximation (MA) approach proposed in [59]. A Markov approximation framework consists of two steps, log-sum-exp approximation and design of a problem-specific Markov chain. Let $\mathcal{K}_S \in \mathcal{F}$ denote a possible candidate for the active device set, where $\mathcal{F}$ denotes the sample space constructed by all possible nonempty subsets of $\mathcal{K}^{all}$ with $|\mathcal{F}| = 2^{|\mathcal{K}^{all}|} - 1$. Following the framework, we aim to obtain the optimal probability of choosing $\mathcal{K}_S \in \mathcal{F}$ as

$$p_{\mathcal{K}_S}^* = \frac{\exp(-\varrho T_{total}^*(\mathcal{K}_S))}{\sum_{\mathcal{K}\in\mathcal{F}} \exp(-\varrho T_{total}^*(\mathcal{K}))}, \tag{43}$$

where $\varrho \geq 0$ is a constant. However, it is challenging to compute $T_{total}^*(\mathcal{K}) = \Psi^\star(\mathcal{K}) G\left(\kappa + \frac{1}{|\mathcal{K}|}\right)$ with the optimal value $\Psi^\star(\mathcal{K})$ for each $\mathcal{K} \in \mathcal{F}$. Thus, we design a Markov chain for the problem, in which the states are defined by the feasible active device sets $\mathcal{K}_S$ with stationary probability distribution $\{p_{\mathcal{K}_S}^*, \mathcal{K}_S \in \mathcal{F}\}$. Since the feasible candidates will be time-shared according to $p_{\mathcal{K}_S}^*$ when the Markov chain converges, the candidates with low total latency will have high probabilities and candidates are selected most of the time. It was proven in [59] that for any probability distribution of the product form $p_{\mathcal{K}_S}^*$ given in (43), there exists at least one time-reversible ergodic Markov chain of which the stationary distribution is given by $p_{\mathcal{K}_S}^*$.

Algorithm 4 MA-based algorithm for active device selection.

1: **Input:** device set $\mathcal{K}^{all}$, κ, G
2: Initialize the current state as $\mathcal{K}_S = \mathcal{K}^{all}$ and compute $T_{total}^*(\mathcal{K}_S)$ through Algorithm 3.
3: Set $l = 1$.
4: **while** $l \leq I_{ma}$ **do**
5: Choose $\mathcal{K}_S'$ randomly such that $\mathcal{K}_S' \subset \mathcal{K}_S$ and $|\mathcal{K}_S'| = |\mathcal{K}_S| - 1$.
6: Compute the total latency $T_{total}^*(\mathcal{K}_S')$ via Algorithm 3.
7: $\mathcal{K}_S^{next} \leftarrow \begin{cases}\mathcal{K}_S' & \text{with probability } q_{\mathcal{K}_S \to \mathcal{K}_S'} \\ \mathcal{K}_S & \text{with probability } 1 - q_{\mathcal{K}_S \to \mathcal{K}_S'}\end{cases}$
8: **if** $\mathcal{K}_S^{next} == \mathcal{K}_S$ **then**
9: $l \leftarrow l + 1$
10: **else**
11: $\mathcal{K}_S \leftarrow \mathcal{K}_S'$, $T_{total}^*(\mathcal{K}_S) \leftarrow T_{total}^*(\mathcal{K}_S')$.
12: $l = 1$
13: **end if**
14: **end while**
15: **Output:** $\mathcal{K}^\star = \mathcal{K}_S$ and $T_{total}^\star = T_{total}^*(\mathcal{K}_S)$.

Let candidates $\mathcal{K}_S$ and $\mathcal{K}_S'$ be states of time-reversible ergodic Markov chain with stationary distribution $p_{\mathcal{K}_S}^*$. To allow a large degree of freedom in the algorithm design, the following two assumptions are sufficient: 1) any two states are reachable from each other, and 2) all $\mathcal{K}_S$, $\mathcal{K}_S' \in \mathcal{F}$ satisfy the balanced equation:

$$p_{\mathcal{K}_S}^* q_{\mathcal{K}_S \to \mathcal{K}_S'} = p_{\mathcal{K}_S'}^* q_{\mathcal{K}_S' \to \mathcal{K}_S} \tag{44}$$

where $q_{\mathcal{K}_S \to \mathcal{K}_S'}$ and $q_{\mathcal{K}_S' \to \mathcal{K}_S}$ are the transition probabilities of $\mathcal{K}_S \to \mathcal{K}_S'$ and $\mathcal{K}_S' \to \mathcal{K}_S$, respectively. Based on (44), we have

$$\begin{aligned} q_{\mathcal{K}_S \to \mathcal{K}_S'} &= \frac{\exp(-\tau)}{1+\exp[-\varrho(T_{total}^*(\mathcal{K}_S) - T_{total}^*(\mathcal{K}_S'))]} \\ q_{\mathcal{K}_S' \to \mathcal{K}_S} &= \frac{\exp(-\tau)}{1+\exp[-\varrho(T_{total}^*(\mathcal{K}_S') - T_{total}^*(\mathcal{K}_S'))]} \end{aligned} \tag{45}$$

where τ is a constant. From this property, the MA-based device selection algorithm is devised and summarized in Algorithm 4 in which we allow $\mathcal{K}_S' \subset \mathcal{K}_S$ and $|\mathcal{K}_S'| = |\mathcal{K}_S| - 1$ to satisfy the two assumptions and I_{ma} is the allowed number of choosing the same candidate in sequence. The algorithm outputs $\mathcal{K}^\star$ and the total latency $T_{total}^\star$ of FL training for the solution of problem **BS-IRS** for a given IRS subset.

C. Complexity of Algorithms

For given K and $L = |\mathcal{L}|$, the AO iteration in Algorithm 3 (from line 4 to line 9) performs Algorithm 1 at $\mathcal{O}(I_{sca} K^3)$ and Algorithm 2 at $\mathcal{O}(I_{fea}(LN)^{4.5})$ with I_{fea} iterations of solving (PI2b) [28]. The complexity of Algorithm 3 performing AO up to I_{ord} times is upper bounded as

$\mathcal{O}((I_{sca}K^3 + I_{fea}(LN)^{4.5})I_{ord})$. Thus, the total complexity of Algorithm 4 is upper bounded as $\mathcal{O}((I_{sca}|\mathcal{K}^{all}|^3 + I_{fea}(LN)^{4.5}|)I_{ord}I_{ma}|\mathcal{K}^{all}|)$ since Algorithm 4 runs Algorithm 3 up to $|\mathcal{K}^{all}|I_{ma}$ iterations.

IV. Auction Design for IRS Allocation

A. IRS Auction Model

As described in Section II-A, an IRS provider provides the IRSs for the BSs in proximity which are operating in distinct frequency bands licensed to different service providers. An IRS can associate with any connected BS. The BSs compete with one another for the IRS-assisted FL, which is modeled by an auction in this paper. In this proposed auction, an IRS provider acting as a seller and also as an auctioneer receives the bids from multiple BSs and decides the set of IRSs allocated to each BS through the auction winner determination. The auction process can be summarized as follows.

In Stage I, each BS evaluates the values of the IRS subsets in assisting the FL training, and submits the bids for the IRS subsets to the auctioneer. Each BS m can submit multiple bids for different IRS subsets as $\mathcal{B}_m = \{\mathfrak{b}_m^i\}_{i=1}^{B_m}$, where B_m denotes the total number of bids submitted by BS m and $\mathfrak{b}_m^i = \{\mathcal{L}_m^i, b_m(\mathcal{L}_m^i)\}$ is the ith bid of BS m consisting of IRS subset $\mathcal{L}_m^i$ and its bidding price $b_m(\mathcal{L}_m^i)$. Here, the bidding price is determined as $b_m(\mathcal{L}_m^i) = 1/T^{\star}_{total|\mathcal{L}_m^i}$, where $T^{\star}_{total|\mathcal{L}_m^i}$ is the total training latency of BS m with the help of $\mathcal{L}_m^i$ assessed by Algorithm 4. It implies that an IRS subset with a longer total training latency is less valuable. The set of all bids submitted to the auctioneer is denoted by $\mathcal{B} = \underset{m\in\mathcal{M}}{\cup}\mathcal{B}_m$. In Stage II, based on the bids submitted by the BSs, the auctioneer determines the winning BS of each IRS and the corresponding payment so that the total social welfare is maximized.

After the auction results are released, each BS initiates its FL session with the help of the allocated IRSs. Each BS pays its assistant IRSs when the FL session ends. A BS possibly bids untruthfully to achieve a higher utility which may adversely affect the social welfare. To address this issue, we propose the winner and payment determination methods that force bidding with the true value to become a dominant strategy for the BSs in the following.

B. Winner Determination

Let $\mathcal{J} = \{J_m^i, i = 1, 2, \cdots, B_m, m \in \mathcal{M}\}$ denote the set of the association/winner indicators, where $J_m^i = 1$ if the ith bid of BS m wins and $J_m^i = 0$, otherwise. The utility U_m^i of bid $\mathfrak{b}_m^i = \{\mathcal{L}_m^i, b_m(\mathcal{L}_m^i)\}$ is defined as the difference between the valuation $b_m(\mathcal{L}_m^i)$ and the payment q_m^i, if this bid wins. Otherwise, the utility U_m^i equals zero. The utility of all BSs participating in the IRS auction is given by $U_{BS} = \sum_{m,i}\big(b_m(\mathcal{L}_m^i) - q_m^i\big)J_m^i$ while the utility of the auctioneer is given by the sum of payments of all winning bidders as $U_{auct} = \sum_{m,i} J_m^i q_m^i$. The social welfare is the sum of utilities of all BSs and the auctioneer, which is the sum of bidding prices of all bidders. Based on the bids collected from the BSs, the auctioneer determines the winning BS of each IRS to maximize the social welfare. Thus, the winner determination problem (WDP) can be formulated as

Algorithm 5 Greedy algorithm for WDP.

while $\mathcal{L}_U \neq \emptyset$ AND $\sum_{m,i} J_m^i < |\mathcal{M}|$ **do**
  $(m^*, i^*) = \arg\max_{(m,i)} \frac{b_m(\mathcal{L}_m^i)}{|\mathcal{L}_m^i|+a}$.
  $J_{m^*}^{i^*} = 1$.
  $b_{m^*}(\mathcal{L}_{m^*}^i) = 0, \forall i \in \mathcal{B}_{m^*}$.
  $\mathcal{L}_S \leftarrow \mathcal{L}_S \cup \mathcal{L}_{m^*}^{i^*}$.
  $\mathcal{L}_U \leftarrow \mathcal{L}_U \setminus \mathcal{L}_{m^*}^{i^*}$.
  for each bid $\{\mathcal{L}_m^i, b_m(\mathcal{L}_m^i)\}$ **do**
    if $(\mathcal{L}_S \bigcap \mathcal{L}_m^i \neq \emptyset)$ **then**
      Set $b_m(\mathcal{L}_m^i) = 0$.
    end if
  end for
end while

$$\text{(WDP)}: \quad \max_{\mathcal{J}} \sum_{m,i} J_m^i b_m(\mathcal{L}_m^i) \tag{46}$$

$$\text{s.t.} \quad \sum_{i=1}^{B_m} J_m^i \leq 1,\ m \in \mathcal{M}, \tag{46a}$$

$$\sum_{(m,i):\ l\in\mathcal{L}_m^i} J_m^i \leq 1,\ l \in \mathcal{L}^{all}, \tag{46b}$$

$$J_m^i \in \{0, 1\}. \tag{46c}$$

where (46a) implies that each BS m can win at most one bid while (46b) implies that each IRS l can assist at most one BS.

We implement a polynomial-time greedy algorithm to obtain an approximate optimal solution for the WDP with single-minded bidders. The main idea of the greedy algorithm is to allocate the IRS to the bidder with the highest normalized value of the bid defined as $\frac{b_m^i}{|\mathcal{C}_m^i|+a}$, where a is a constant determined by the designer. The intuition here is that if a is small, then the auctioneer will tend to choose the bid with smaller $|\mathcal{C}_m^i|$ as the winner, which make IRSs underutilized. Meanwhile if a is larger, the worst case is selecting winner based on the value of bid, which can be regarded as the second-price auction. The details of the greedy algorithm are presented in Algorithm 5.

Remark: The WDP (46) is formulated for a scenario where the IRS provider deploys sufficient IRSs in supporting neighboring BSs. Nonetheless, to support a small number of large size IRSs more effectively, it can be modified by addressing a virtual IRS concept. This concept divides an IRS into multiple virtual IRSs constructed by disjoint subgroups of adjacent elements. The WDP (46) is then formulated with virtual IRSs acting as IRSs and is solved with Algorithm 5.

C. Payment Determination

The design of a pricing scheme is of critical importance to achieving truthfulness. We adopt the procedure in [46] to determine the payment for winning bidder $\mathfrak{b}_m^i = \{\mathcal{L}_m^i, b_m(\mathcal{L}_m^i)\}$ of BS m by taking into account the loss incurred by selecting the winning bidder $\mathfrak{b}_m^i$. We consider each bid as a virtual bidder. For the payment, we find new winning bidders by running algorithm 5 after removing the winning bidder $\mathfrak{b}_m^i$,

or equivalently with the set $\mathcal{B} \setminus \{\mathfrak{b}_m^i\}$ of bids for the input. This output is denoted by $\mathcal{J}_{-m,-i}$ which is referred to as the bidder blocked by bidder $\mathfrak{b}_m^i$ since they cannot win when bidder $\mathfrak{b}_m^i$ participates in the auction. Let $\mathcal{C}^\star_{-m,-i}$ denote the set of indices (m', i') corresponding to the winning bidders blocked by bidder $\mathfrak{b}_m^i$; i' is the index of the winning bid of BS m' blocked by bidder $\mathfrak{b}_m^i$. Then, the greedy price for winning bidder $\mathfrak{b}_m^i$ is determined by

$$q_m^{i,\text{greedy}} = \max_{(m',i')\in\mathcal{C}^\star_{-m,-i}} \frac{b_{m'}(\mathcal{L}_{m'}^{i'})}{|\mathcal{L}_{m'}^{i'}|+a}(|\mathcal{L}_m^i|+a) \tag{47}$$

In some cases, the resulting revenue of the IRS provider can be even far from the optimal one. As an extreme case, the price of each bidder is zero if the blocked bid set is empty for all winners. To avoid this situation, the IRS provider introduces the base price q^{base} and charges the winning BS m the price no less than the base price as follows:

$$q_m^i = \max\{q^{\text{base}}, q_m^{i,\text{greedy}}\}. \tag{48}$$

D. Properties

We define some economic attributes describing an auction mechanism and then present important properties of the designed auction mechanism for IRS allocation.

Definition 1. *(Truthfulness) An auction mechanism is truthful if and only if for every bidder $\mathfrak{b}_m^i = \{\mathcal{L}_m^i, b_m(\mathcal{L}_m^i)\}$ can receive the highest utility when it reports true value.*

To analyze the truthfulness of the proposed mechanism, we first introduce the concepts of monotone and critical value as follows:

Definition 2. *(Monotonicity) The allocation scheme of an auction is L-monotone if bid $\mathfrak{b}_m^i = \{\mathcal{L}_m^i, b_m(\mathcal{L}_m^i)\}$ is a winning bidder, then all bidders with $\mathfrak{b}_{m'}^{i'} \succeq \mathfrak{b}_m^i$ are also winning bidders, where $\succeq$ denotes the preference of the bidders defined as follows: $\{\mathcal{L}_{m'}^{i'}, b_{m'}(\mathcal{L}_{m'}^{i'}\} \succeq \{(\mathcal{L}_m^i, b_m(\mathcal{L}_m^i))\}$ when $b_{m'}(\mathcal{L}_{m'}^{i'}) \geq b_m(\mathcal{L}_m^i)$ for $|\mathcal{L}_{m'}^{i'}| = |\mathcal{L}_m^i|$ and $|\mathcal{L}_{m'}^{i'}| \leq |\mathcal{L}_m^i|$ for $b_{m'}(\mathcal{L}_{m'}^{i'}) = b_m(\mathcal{L}_m^i)$.*

Definition 3. *(Critical value) For a given monotone allocation scheme, there exists a critical value $\hat{q}_m^i$ of each bidder $\{\mathcal{L}_m^i, b_m(\mathcal{L}_m^i)\}$ such that $b_m(\mathcal{L}_m^i) \geq \hat{q}_m^i$ will be a winning bidder while $b_m(\mathcal{L}_m^i) \leq \hat{q}_m^i$ is a losing bidder.*

The critical value can be regarded as the minimum value that a bidder should bid to obtain the requested IRS subset. With the notion of monotonicity and critical value, we have the following lemmas.

Lemma 1. *An auction mechanism is truthful if the allocation scheme is monotone and each winning bidder pays the critical value.*

Proof. The proof is immediate from Lemma 1 and Theorem 1 in [60]. □

We now prove that the winner determination algorithm 5 is monotone and the payment determined for a winner BS is the critical value of its bid.

Lemma 2. *The winner determination algorithm 5 is monotone.*

Proof. Algorithm 5 is monotone from line 2 since $\frac{b_{m'}(\mathcal{L}_{m'}^{i'})}{|\mathcal{L}_{m'}^{i'}|+a} \geq \frac{b_m(\mathcal{L}_m^i)}{|\mathcal{L}_m^i|+a}$ when $b_{m'}(\mathcal{L}_{m'}^{i'}) \geq b_m(\mathcal{L}_m^i)$ for $|\mathcal{L}_{m'}^{i'}| = |\mathcal{L}_m^i|$ and $|\mathcal{L}_{m'}^{i'}| \leq |\mathcal{L}_m^i|$ for $b_{m'}(\mathcal{L}_{m'}^{i'}) = b_m(\mathcal{L}_m^i)$. It is clear that a BS can increase its chance of winning by increasing its bid or decreasing the number of desired IRSs. □

Lemma 3. *q_m^i is a critical value for each winning bidder $\{\mathcal{L}_m^i, b_m(\mathcal{L}_m^i)\}$.*

Proof. We consider two cases of winning bidder $\{\mathcal{L}_m^i, b_m(\mathcal{L}_m^i)\}$, where $b_m(\mathcal{L}_m^i) \leq q_m^i$ or $b_m(\mathcal{L}_m^i) > q_m^i$.

Case 1: If bidder $\{\mathcal{L}_m^i, b_m(\mathcal{L}_m^i)\}$ wins with bidding price $b_m(\mathcal{L}_m^i) \leq q_m^i$, we have either $b_m(\mathcal{L}_m^i) \leq q^{\text{base}}$ or $b_m(\mathcal{L}_m^i) \leq q_m^{i,\text{greedy}}$. If $b_m(\mathcal{L}_m^i) \leq q_m^{i,\text{greedy}}$, we have $b_m(\mathcal{L}_m^i) \leq \max_{(\mathcal{L}_{m'}^{i'}, b_{m'}(\mathcal{L}_{m'}^{i'}))\in\mathcal{B}^\star_{-m,-i}} \frac{b_{m'}(\mathcal{L}_{m'}^{i'})}{|\mathcal{L}_{m'}^{i'}|+a}(|\mathcal{L}_m^i|+a)$. Thus, bidder $\{\mathcal{L}_m^i, b_m(\mathcal{L}_m^i)\}$ cannot win the bid. If $b_m(\mathcal{L}_m^i) \leq q^{\text{base}}$, bidder $\{\mathcal{L}_m^i, b_m(\mathcal{L}_m^i)\}$ can not attend the auction.

Case 2: If bidder $\{\mathcal{L}_m^i, b_m(\mathcal{L}_m^i)\}$ wins with bidding price $b_m(\mathcal{L}_m^i) > q_m^i$, we have either $b_m(\mathcal{L}_m^i) > q^{\text{base}}$ or $b_m(\mathcal{L}_m^i) > q_m^{i,\text{greedy}}$. Then, the bidder can attend the auction and becomes the winner from line 2 of Algorithm 5. □

From Lemmas 1-3, we finally conclude that the proposed mechanism with the critical value given by $\hat{q}_m^i = q_m^i$ is a truthful mechanism.

E. Complexity and Convergence

The complexity of Algorithm 5 is dominated by finding the maximum value of the normalized valuation (line 2) computed at complexity $\mathcal{O}(B_T)$ for the total number B_T of bids submitted by all the BSs. Thus, the complexity of Algorithm 5 5is given by $\mathcal{O}(|\mathcal{M}|T\log_2 B_T)$ to find the maximum value for $|\mathcal{M}|$ BSs and is solvable in polynomial time. In addition, since the number of submitted bids and the number of IRSs are limited, the greedy algorithm for WDP converges.

V. Performance Evaluation

We first investigate the time latency of one training round and the total latency of the FL with the proposed algorithms. We then evaluate the performance of the proposed auction scheme utilizing the optimized total latency for the bids.

A. Simulation Conditions

The training performance of the FL is evaluated with the well-known learning task, handwritten digit classification using the MNIST dataset. The MNIST dataset consists of $60,000$ training images and $10,000$ testing images of the 10 digits [61]. To construct both iid and non-iid local training datasets, we follow a method similar to that of [55] in allocating 3000 training images to each device after dividing the training images of each digit into 20 shards of 300 images; Each device is assigned 10 shards, where ξ shards are from the same digit and $10-\xi$ shards are from different digits for $0 \leq \xi \leq 10$. We refer ξ as the non-iid level since the irregularity of the

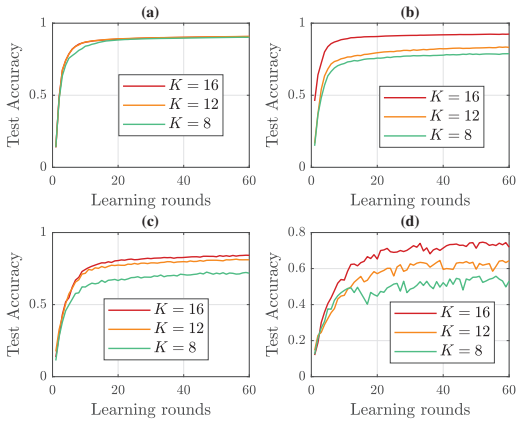

Fig. 3: Test accuracy as a function of the number of learning rounds when the datasets are (a) iid with $\xi = 0$, (b) non-iid with $\xi = 5$, (c) non-iid with $\xi = 7$, and (d) non-iid with $\xi = 9$.

TABLE II: Estimated values on G and κ for the number of rounds to attain 67% accuracy.

Non-iid level	$\xi = 0$	$\xi = 2$	$\xi = 5$	$\xi = 7$	$\xi = 9$
G	12.02	34.00	62.00	208.6	776.0
κ	0.2436	0.0440	-0.0024	-0.0347	-0.0370

local dataset increases as ξ increases. For local training, each device implements a feedforward neural network (FNN) with one hidden layer of 64 neurons followed by ReLU activation. Thus, the FNN consists of $50,890$ weights in total which are represented with $S_\omega = 3$ Mbits. For each local training, we set $\eta = 0.01$, $d_{mk} = 128$, and $\mathsf{I}_u = 2$ for the learning rate, minibatch size, and number of model updates, respectively. The computational latency is generated by following the model in (8) with $\iota_{mk} \sim \text{Unif}[5 \times 10^8, 10^9]$ CPU-cycles/second and $\nu = 6 \times 10^5$ CPU-cycles/sample.

To estimate G and κ for the total latency in (20), we investigate the convergence behavior of the test accuracy in FL using the local training datasets of different non-iid level ξ in Fig. 3. Although the test accuracy is almost identical irrespective of the number K of active devices for the iid datasets with $\xi = 0$, a larger number K of active devices improves the test accuracy more as the non-iid level ξ increases. With the results, we obtain G and κ for different values of ξ in Table II, which will be employed for the total latency.

For the wireless network, we assume $B_u = 10$ MHz for the uplink bandwidth of each BS in providing its own FL service at a different frequency band, $\sigma^2 = -124$ dBm for the noise power at the BS, $P_0 = 100$ mW for the maximum transmit power of the device, and $R_{\min} = 200$ kbps for the minimum required rate of each device. The channel models include path loss and Rayleigh fading. The path loss at distance d is modeled by $L(d) = 10^{-3} d^{-\alpha}$ with path loss exponent α [58], which is set to 4, 2.6, and 2.2 for the BS-device, IRS-device, and BS-IRS links, respectively. The positions of the nodes are specified on the (x, y) coordinates given in meters.

B. Performance with Latency Minimizing Algorithms

This subsection evaluates the latency and training performances of the proposed algorithms for a single BS. The BS is located at the origin and the IRSs are located at $(20, -20)$, $(15, -25)$, and $(25, -15)$, unless otherwise specified, which are turned on in sequence according to the number L of IRSs.

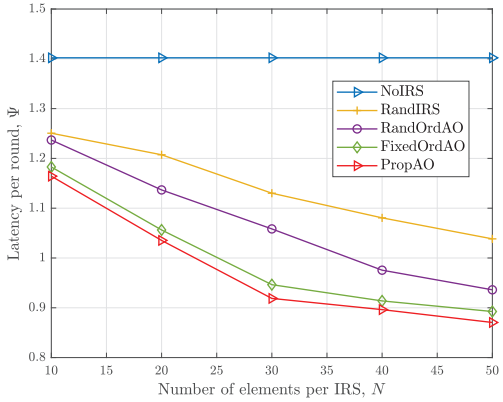

Fig. 4: Latency per training round as the number N of IRS elements increases when $L = 1$.

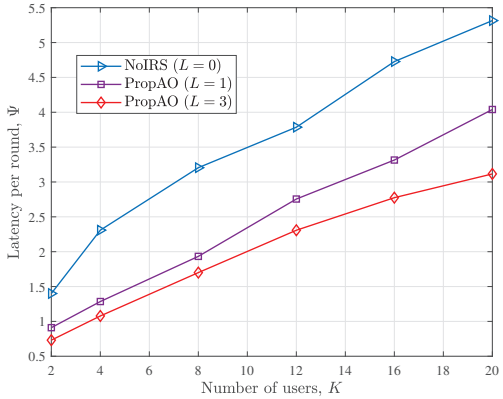

Fig. 5: Latency per training round as the number K of active devices increases when $N = 30$.

For FL with the IRS-assisted NOMA, the latency Ψ per training round is provided in Fig. 4 as the number N of IRS elements increases when $L = 1$ and two devices located at $(499, -491)$ and $(358, -390)$ are active. In the figure, PropAO denotes the results with the proposed algorithm 3 with $I_{ord} = 3$ while NoIRS, RandIRS, RandOrdAO and FixedOrdAO correspond to the results with a reduced form of the proposed algorithm without IRS, with random IRS phases, with a random decoding order, and with only the initial decoding order ($I_{ord} = 1$), respectively. The training latency decreases as the number N of IRS elements increases. The proposed algorithm improves the latency by about 43 % when compared with NoIRS. In addition, the channel-power based decoding order (FixedOrdAO) improves the performance compared with random selection of a decoding order and PropAO improves the latency of FixedOrdAO further through updating the decoding order and selecting the best outcome.

Fig. 5 demonstrates the latency per training round as the number K of active devices increases when the number of IRSs is set to $L = 0$, 1, and 3 with $N = 30$. The devices are uniformly distributed in the cell of radius $r = 500$ m. The latency per round increases as the number of active devices

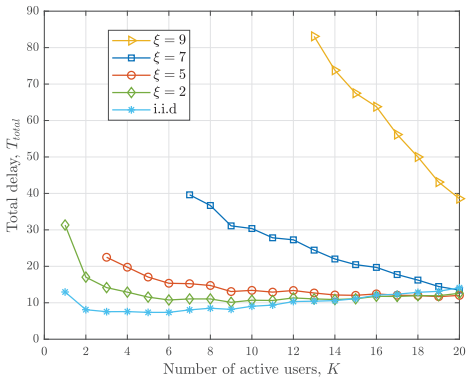

Fig. 6: Total delay T_{total} in achieving 67 % accuracy as the number K of active devices increases when $L = 1$ and $N = 30$.

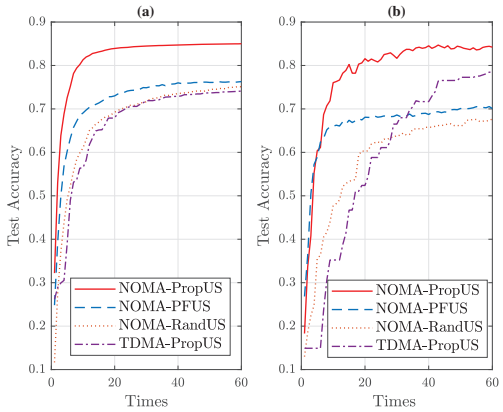

Fig. 7: Test accuracy of different device selection policies as the training time elapses: (a) $\xi = 2$ (b) $\xi = 7$.

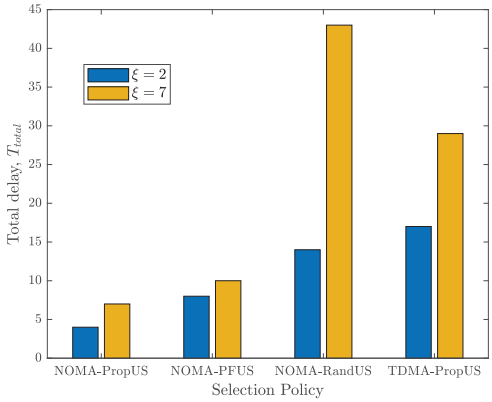

Fig. 8: Total delay of different device selection policies in attaining the test accuracy of 67 %.

increases since each device rate decreases by sharing the same wireless resource and the worst-case device dominates the performance. On the other hand, more IRSs reduce the latency per round by transforming wireless channel environments more suitable for the FL metric.

Fig. 6 provides the total delay T_{total} as the number K of active devices increases with $L = 1$ and $N = 30$ as in Fig. 5 and the datasets with non-iid level ξ in Table II are used. When K is small, the total delay increases significantly as the non-iid level ξ increases. However, the total delay decreases rapidly by increasing the number of active devices, which reduces the number of training rounds required to obtain a given accuracy level. The results reveal a tradeoff between the learning efficiency improved by allowing more devices in FL as observed in Fig. 3 and the communication delay increased by allowing more devices as observed in Fig. 5. Henceforth, there exists an optimal number of active devices that minimizes the total delay for each non-iid level. For instance, the optimal number of active devices is observed to be about $K = 6$ and 19 for $\xi = 2$ and 5, respectively.

We next provide the overall performance with active device selection when $L = 3$, $N = 10$, and $|\mathcal{K}^{all}| = 20$. We provide the test accuracy with respect to the wallclock time in Fig. 7 when the non-iid level is $\xi = 2$ in Fig. 7(a) and $\xi = 7$ in Fig. 7(b). Here, NOMA-PropUS denotes Algorithm 4 combined with Algorithm 3, where $\varrho = 500$ and $I_{ma} = 50$. NOMA-PFUS and NOMA-RandUS apply Algorithm 3 after selecting $K = 8$ active devices through the proportional fair (PF) method [62] and in a random way, respectively. TDMA-PropUS denotes TDMA with equal time allocation applying a greedy device selection similar to Algorithm 4.

Fig. 7 shows that NOMA-PropUS outperforms the other baseline schemes in both the convergence rate and converged test accuracy. Specifically, NOMA-PropUS improves the test accuracy at time 60 s by about 11 % over TDMA-PropUS and by about 21 % over NOMA-RandUS/NOMA-PFUS when $\xi = 7$ while by about 15 % over the other schemes when $\xi = 2$. This improvement results from the fact that NOMA-PropUS incorporates both the computation and communication delays in device selection while NOMA-PFUS incorporates only the communication delay and NOMA-RandUS does not include either of them. The gain of NOMA-PropUS over TDMA-PropUS is due to the advantage of NOMA over TDMA in resource utilization.

The total delay T_{total} to attain an accuracy in Fig. 7 is provided in Fig. 8 when $\xi = 2$ and $\xi = 7$. The accuracy is set to 67 %, which is the highest accuracy of NOMA-RandUS when $\xi = 7$. The results confirm that NOMA-PropUS provides the lowest total delay by providing a better tradeoff between the latency per round and the number of training rounds required to achieve a given accuracy.

C. Performance with Auction

This subsection provides the performance of the proposed auction with $M = 4$ BSs, $|\mathcal{L}^{all}| = 10$ IRSs each with $N = 10$ elements, and $|\mathcal{K}_m^{all}| = 10$ devices per BS, positioned as in Fig. 9, unless stated otherwise. The number of bids submitted by each BS is set to be identical for all BSs as $B_m = B$ and the non-iid level of local datasets is set to $\xi = 7$.

The social welfare with the proposed winner determination algorithm is shown as the number B of bids per BS increases in Fig. 10 when the IRS subsets $\mathcal{L}_m^i$ in the bids are constructed by changing the number of requested IRSs as $|\mathcal{L}_m^i| = \max(5-i, 1)$ for $i = 1, 2, \cdots, B$. Fig. 10(a) compares the performance of the proposed method and benchmarks for multiple IRSs as in Fig. 9. OptWD denotes the optimal

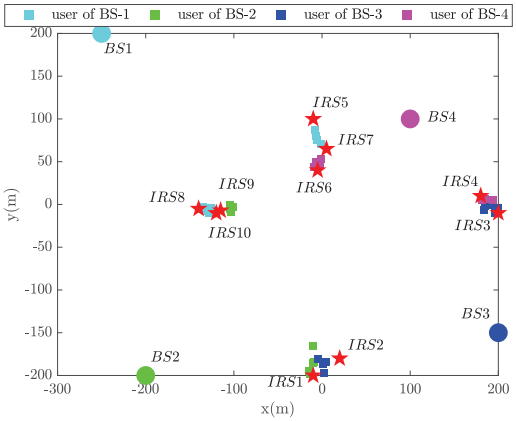

Fig. 9: Location of BSs, IRSs, and devices.

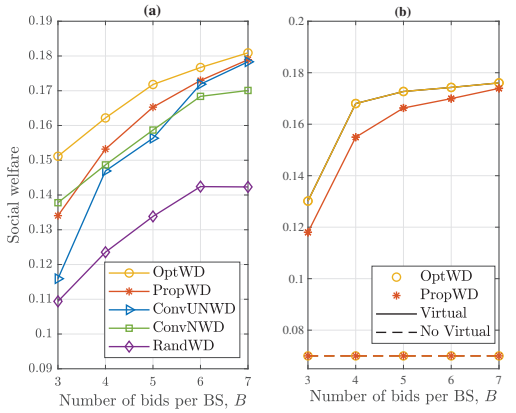

Fig. 10: Social welfare as the number B of bids increases when the bids consist of the IRS subsets of nonuniform size: (a) multiple IRSs and (b) virtual IRSs for a single IRS.

solution obtained by the exhaustive search, PropWD denotes the proposed method using Algorithm 5 with $a = 160$, and RandWD denotes the random IRS selection. ConvNWD and ConvUNWD are the greedy algorithms allocating the IRSs with $b_m^i(\mathcal{L}_m^i)$ (without normalization) [46] and with $\frac{b_m^i(\mathcal{L}_m^i)}{|\mathcal{L}_m^i|}$ (with normalization), respectively. The social welfare increases as the number B of bids increases since there are more chances for selecting the winners with higher bid values. PropWD provides the second-best social welfare following OptWD in most cases. Fig. 10(b) provides the social welfare of the proposed method with and without virtual IRS concept when only a single IRS with 100 elements is available at location $(-50, 0)$ instead of multiple IRSs in Fig. 9. Virtual denotes the results when 10 virtual IRSs with 10 elements created from a single IRS are allocated while No Virtual denotes the results when a single IRS is allocated. It is shown that the social welfare can be improved substantially by constructing the virtual IRSs when only a small number of IRSs are available.

We also compare the auction performance achieved with the bids when the size of the IRS subsets is limited for practical the implementation in Fig. 11. The social welfare of the network is provided as the number B of bids increases in Fig. 11(a) and the corresponding numbers of satisfied BSs and allocated IRSs are provided in Figs. 11(b) and 11(c), respectively. Here, Single-IRS, Double-IRS, Mixed-IRS construct the IRS subsets in the bids with $|\mathcal{C}_m^i| = 1$, $|\mathcal{C}_m^i| = 2$, and $|\mathcal{C}_m^i| = 1$ or 2, respectively. Fig. 11(a) shows that the social welfare improves as the number of bids per BS increases since the auctioneer has more opportunities to select the winning bids with higher bid values. Single-IRS outperforms Double-IRS for a small B while vice versa for a large B. Mixed-IRS lies between the performances of Single-IRS and Double-IRS. When the number of bids is small, Single-IRS provides a better social welfare than Double-IRS since the IRS subsets desired by the BSs can overlap each other for Double-IRS. As a result, all BSs are not satisfied with Double-IRS when $B \leq 2$ although all BSs are satisfied with Single-IRS as observed in Fig. 11(b). When the number B of bids is larger than 3, the social welfare attained with Double-IRS gets larger than that with Single-IRS in Fig. 11(a) since more IRSs can be utilized with Double-IRS as shown in Fig. 11(c). In addition, all BSs can obtain their desired IRS subsets as shown in Fig. 11(b) when $B \geq 3$.

VI. Conclusion

This paper has considered a business model of an IRS provider that deploys multiple IRSs to assist the FL applications of neighboring BSs of different operators employing uplink NOMA. Our goal is to minimize the total training latency of each BS by allocating IRSs and optimizing the IRS and NOMA parameters. Firstly, assuming that a subset of IRSs is allocated, we have proposed the algorithm optimizing IRS reflection and power allocation jointly for a suboptimal decoding order for NOMA to minimize the latency per round, which is combined with the device selection to minimize the total latency. Next, we have provided an auction mechanism between an IRS provider and the BSs for IRS allocation with the optimized total latency. For the auction, we have proposed a greedy algorithm to solve the NP-hard winner selection problem and payment scheme to ensures truthfulness, individual rationality.

The results have shown that the proposed IRS-NOMA optimization algorithm reduces the latency per round and improves the FL performance when combined with device selection. Specifically, it was observed that the proposed method improves the test accuracy by about 11 % and reduces the total delay by 57 % when compared with the TDMA counterpart for a non-iid local data model. Finally, the effectiveness of the proposed auction mechanism was demonstrated by showing that the proposed winner determination outperforms the other conventional algorithms. It was also observed that the social welfare gets improved when a BS constructs a bid on multiple IRSs and the number of bids submitted by a BS increases.

Appendix

We provide a convergence analysis of the FL model owned by a BS provided in Section II-B after ignoring the subscript m denoting the BS index. The FL optimization problem (2) with (3) is then expressed as

$$\min_{\boldsymbol{\omega}} \left[F(\boldsymbol{\omega}) \triangleq \sum_{k \in \mathcal{K}} \varepsilon_k F_k(\boldsymbol{\omega}) \right], \tag{49}$$

where $\varepsilon_k = D_k/D$ with $F_k(\boldsymbol{\omega}) = \frac{1}{D_k} \sum_{d=1}^{D_k} f(\boldsymbol{\omega}; \mathbf{x}_{kd}, \mathbf{y}_{kd})$. The analysis is obtained by using the results obtained in [14] under the following assumptions.

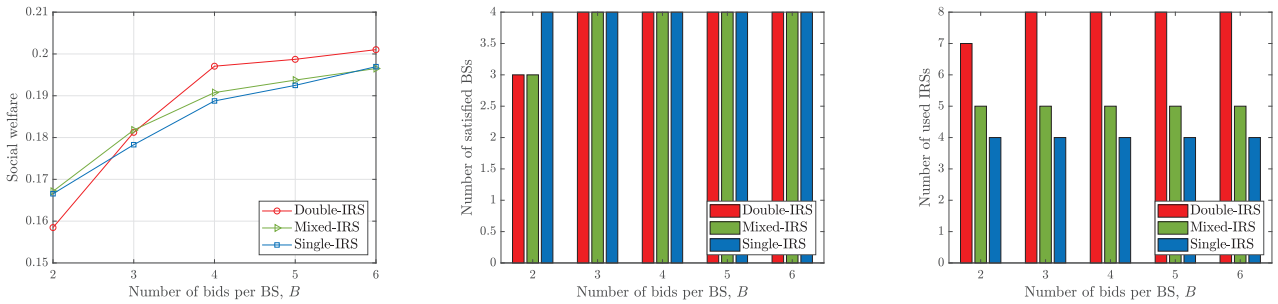

(a) (b) (c)

Fig. 11: Auction performance as the number B of bids per BS increases; (a) social welfare (b) number of satisfied BSs (c) number of allocated IRSs.

Assumption 1. *Assume $F_k, k \in \mathcal{K}$ are L-smooth; for all $\boldsymbol{v}$ and $\boldsymbol{\omega}$, $F_k(\boldsymbol{v}) \leq F_k(\boldsymbol{\omega}) + (\boldsymbol{v}-\boldsymbol{\omega})^T \nabla F_k(\boldsymbol{\omega}) + \frac{\mathsf{L}}{2}\|\boldsymbol{v}-\boldsymbol{\omega}\|^2$.*

Assumption 2. *Assume $F_k, k \in \mathcal{K}$ are μ-strongly convex; for all $\boldsymbol{v}$ and $\boldsymbol{\omega}$, $F_k(\boldsymbol{v}) \geq F_k(\boldsymbol{\omega}) + (\boldsymbol{v}-\boldsymbol{\omega})^T \nabla F_k(\boldsymbol{\omega}) + \frac{\mu}{2}\|\boldsymbol{v}-\boldsymbol{\omega}\|^2$.*

Assumption 3. *Let $(\boldsymbol{x}_{kt}, \boldsymbol{y}_{kt})$ be sampled randomly from the local data of device k at time t. The variance of stochastic gradients of device k at time t is bounded as $\mathbb{E}[\|\nabla F_k(\boldsymbol{\omega}_k^t, \boldsymbol{x}_{kt}, \boldsymbol{y}_{kt}) - \nabla F_k(\boldsymbol{\omega}_k^t)\|^2] \leq \varsigma_k^2$ for $k \in \mathcal{K}$.*

Assumption 4. *The expected squared norm of stochastic gradients at time t is uniformly bounded, i.e., $\mathbb{E}[\|\nabla F_k(\boldsymbol{\omega}_k^t, \boldsymbol{x}_{kt}, \boldsymbol{y}_{kt})\|] \leq \mathcal{G}^2,\ k \in \mathcal{K}$.*

Let F^*, F_k^*, and $\boldsymbol{\omega}^*$ denote the optimal solution of F, F_k, and $\boldsymbol{\omega}$, respectively. The optimality gap of the FL model is given as follows.

Theorem 1. *Let $\varkappa = \mathsf{L}/\mu$, $\zeta = \max(8\varkappa, \mathsf{I}_u)$, and learning rate $\eta_t = 2/(\mu(\zeta+t))$. The optimality gap of the FL is derived as*

$$\mathbb{E}[F(\boldsymbol{\omega}^t)] - F^* = \frac{\varkappa}{\zeta + \mathsf{N}_r\mathsf{I}_u - 1}\left(\frac{2B}{\mu} + \frac{\mu\zeta}{2}\mathbb{E}[\|\boldsymbol{\omega}^0 - \boldsymbol{\omega}^*\|^2]\right), \quad (50)$$

where $B = \sum_{k\in\mathcal{K}} \varepsilon_k^2 \varsigma_k^2 + 6\mathsf{L}\Upsilon + 8(\mathsf{I}_u - 1)^2\mathcal{G}^2$ with $\Upsilon = F^* - \sum_{k\in\mathcal{K}} \varepsilon_k F_k^*$ quantifying the non-iid level in local data.

Proof. The proof is immediate from Theorem 1 in [14]. □

For μ-strongly convex F, we have $\|\boldsymbol{\omega}^0 - \boldsymbol{\omega}^*\|^2 \leq \frac{4}{\mu^2}\mathcal{G}^2$ which makes (50) proportional to

$$\mathcal{O}\left(\frac{\sum_{k\in\mathcal{K}} \varepsilon_k^2\varsigma_k^2 + \mathsf{L}\Upsilon + \mathsf{I}_u^2\mathcal{G}^2 + \zeta\mathcal{G}^2}{\mu\mathsf{N}_r\mathsf{I}_u}\right). \quad (51)$$

Therefore, the number of training rounds required to meet a tolerance error is approximated roughly to

$$\mathsf{N}_r \propto \mathsf{I}_u\mathcal{G}^2 + \frac{\sum_k \varepsilon_k^2\varsigma_k^2 + \mathsf{L}\Upsilon + \varkappa\mathcal{G}^2}{\mathsf{I}_u} + \mathcal{G}^2. \quad (52)$$

If we further assume equal participation of the devices as $\varepsilon_k = \frac{1}{|\mathcal{K}|}$ and identical variance as $\varsigma_k^2 = \varsigma^2$ for $k \in \mathcal{K}$, (52) becomes

$$\mathsf{N}_r \propto (\mathsf{I}_u + 1)\mathcal{G}^2 + \frac{1}{|\mathcal{K}|}\frac{\varsigma^2}{\mathsf{I}_u} + \frac{\mathsf{L}\Upsilon + \varkappa\mathcal{G}^2}{\mathsf{I}_u} \quad (53)$$

from $\sum_{k\in\mathcal{K}} \varepsilon_k^2\varsigma_k^2 = \frac{1}{|\mathcal{K}|}\varsigma^2$, which complies with $\mathsf{N}_r = \left(\kappa + \frac{1}{|\mathcal{K}|}\right) G$ in (19) formulated from the experimental results.

REFERENCES

[1] T. Li, A. K. Sahu, A. Talwalkar, and V. Smith, "Federated learning: Challenges, methods, and future directions," *IEEE Signal Process. Mag.*, vol. 37, no. 3, pp. 50–60, May 2020.

[2] S. Niknam, H. S. Dhillon, and J. H. Reed, "Federated learning for wireless communications: Motivation, opportunities, and challenges," *IEEE Commun. Mag.*, vol. 58, no. 6, pp. 46–51, Jun. 2020.

[3] Y. Liu, X. Yuan, Z. Xiong, J. Kang, X. Wang, and D. Niyato, "Federated learning for 6G communications: Challenges, methods, and future directions," *China Commun.*, vol. 17, no. 9, pp. 105–118, Sep. 2020.

[4] Z. Yang, M. Chen, K.-K. Wong, H. V. Poor, and S. Cui, "Federated learning for 6G: Applications, challenges, and opportunities," *Engineering*, vol. 8, pp. 33–41, Jan. 2021.

[5] D. C. Nguyen, M. Ding, P. N. Pathirana, A. Seneviratne, J. Li, D. Niyato, and H. V. Poor, "Federated learning for industrial Internet of things in future industries," *IEEE Wireless Commun.*, vol. 28, no. 6, pp. 192–199, Dec. 2021.

[6] A. M. Elbir and S. Coleri, "Federated learning for channel estimation in conventional and RIS-assisted massive MIMO," *IEEE Trans. Wireless Commun.*, vol. 21, no. 6, pp. 4255–4268, Jun. 2021.

[7] M.-D. Nguyen, S.-M. Lee, Q.-V. Pham, D. T. Hoang, D. N. Nguyen, and W.-J. Hwang, "HCFL: A high compression approach for communication-efficient federated learning in very large scale iot networks," *IEEE Trans. Mobile Compt.*, pp. 1–13, Jul. 2022.

[8] S. R. Pandey, M. N. Nguyen, T. N. Dang, N. H. Tran, K. Thar, Z. Han, and C. S. Hong, "Edge-assisted democratized learning toward federated analytics," *IEEE Internet Things J.*, vol. 9, no. 1, pp. 572–588, Jan. 2021.

[9] T. Nishio and R. Yonetani, "Client selection for federated learning with heterogeneous resources in mobile edge," in *Proc. IEEE Int. Conf. Commun. (ICC)*, Shanghai, China, Jul. 2019, pp. 1–7.

[10] M. Chen, Z. Yang, W. Saad, C. Yin, H. V. Poor, and S. Cui, "A joint learning and communications framework for federated learning over wireless networks," *IEEE Trans. Wireless Commun.*, vol. 1, pp. 269–283, Oct. 2020.

[11] M. Chen, H. V. Poor, W. Saad, and S. Cui, "Convergence time minimization of federated learning over wireless networks," in *Proc. IEEE Int. Conf. Commun. (ICC)*, Dublin, Ireland, Jun. 2020, pp. 1–6.

[12] W. Shi, S. Zhou, and Z. Niu, "Device scheduling with fast convergence for wireless federated learning," in *Proc. IEEE Int. Conf. Commun. (ICC)*, Dublin, Ireland, Jun. 2020, pp. 1–6.

[13] W. Xia, T. Q. Quek, K. Guo, W. Wen, H. H. Yang, and H. Zhu, "Multi-armed bandit-based client scheduling for federated learning," *IEEE Trans. Wireless Commun.*, vol. 19, no. 11, pp. 7108–7123, Jun. 2020.

[14] X. Li, K. Huang, W. Yang, S. Wang, and Z. Zhang, "On the convergence of fedavg on non-iid data," *Proc. of ICLR*, pp. 1–26, 2020.

[15] W. Saad, M. Bennis, and M. Chen, "A vision of 6G wireless systems: Applications, trends, technologies, and open research problems," *IEEE Network*, vol. 34, no. 3, pp. 134–142, Oct. 2019.

[16] H. Tataria, M. Shafi, A. F. Molisch, M. Dohler, H. Sjöland, and F. Tufvesson, "6G wireless systems: Vision, requirements, challenges, insights, and opportunities," *Proc. IEEE*, vol. 109, no. 7, pp. 1166–1199, 2021.

[17] Y. Liu, S. Zhang, X. Mu, Z. Ding, R. Schober, N. Al-Dhahir, E. Hossain, and X. Shen, "Evolution of NOMA toward next generation multiple access (NGMA) for 6G," *IEEE J. Sel. Areas Commun.*, vol. 40, no. 4, pp. 1037–1071, Jan. 2022.

[18] Y. Liu, W. Yi, Z. Ding, X. Liu, O. Dobre, and N. Al-Dhahir, "Application of NOMA in 6G networks: Future vision and research opportunities for next generation multiple access," *arXiv preprint arXiv:2103.02334*, 2021.

[19] Y. Jeong, C. Lee, and Y. H. Kim, "Power minimizing beamforming and power allocation for MISO-NOMA systems," *IEEE Trans. Veh. Technol.*, vol. 68, no. 6, pp. 6187–6191, Apr. 2019.

[20] A. Al-Hilo, M. Shokry, M. Elhattab, C. Assi, and S. Sharafeddine, "Reconfigurable intelligent surface enabled vehicular communication: Joint user scheduling and passive beamforming," *IEEE Trans. Veh. Technol.*, vol. 71, no. 3, pp. 2333–2345, Jan. 2022.

[21] Y. Pan, K. Wang, C. Pan, H. Zhu, and J. Wang, "Sum-rate maximization for intelligent reflecting surface assisted terahertz communications," *IEEE Trans. Veh. Technol.*, vol. 71, no. 3, pp. 3320–3325, Jan. 2022.

[22] L. Blumrosen and N. Nisan, "Algorithmic game theory," *Introduction to Mechanism Design, Cambridge University Press, New York, USA*, 2007.

[23] B. Zheng, Q. Wu, and R. Zhang, "Intelligent reflecting surface-assisted multiple access with user pairing: NOMA or OMA?" *IEEE Commun. Lett.*, vol. 24, no. 4, pp. 753–757, Apr. 2020.

[24] F. Fang, Y. Xu, Q.-V. Pham, and Z. Ding, "Energy-efficient design of IRS-NOMA networks," *IEEE Trans. Veh. Technol.*, vol. 69, no. 11, pp. 14 088–14 092, Nov. 2020.

[25] X. Mu, Y. Liu, L. Guo, J. Lin, and N. Al-Dhahir, "Exploiting intelligent reflecting surfaces in NOMA networks: Joint beamforming optimization," *IEEE Trans. Wireless Commun.*, vol. 19, no. 10, pp. 6884–6898, Oct. . 2020.

[26] ——, "Capacity and optimal resource allocation for IRS-assisted multi-user communication systems," *IEEE Trans. Commun.*, vol. 69, no. 6, pp. 3771–3786, Jun. 2021.

[27] Z. Zhang, C. Zhang, C. Jiang, F. Jia, J. Ge, and F. Gong, "Improving physical layer security for reconfigurable intelligent surface aided NOMA 6G networks," *IEEE Trans. Veh. Technol.*, vol. 70, no. 5, pp. 4451–4463, 2021.

[28] B. Yang, X. Cao, C. Huang, C. Yuen, L. Qian, and M. Di Renzo, "Intelligent spectrum learning for wireless networks with reconfigurable intelligent surfaces," *IEEE Trans. Veh. Technol.*, vol. 70, no. 4, pp. 3920–3925, May 2021.

[29] Y. Cheng, K. H. Li, Y. Liu, K. C. Teh, and G. K. Karagiannidis, "Non-orthogonal multiple access (NOMA) with multiple intelligent reflecting surfaces," *IEEE Trans. Wireless Commun.*, vol. 20, no. 11, pp. 7184–7195, Nov. 2021.

[30] M. Zeng, X. Li, G. Li, W. Hao, and O. A. Dobre, "Sum rate maximization for IRS-assisted uplink NOMA," *IEEE Commun. Lett.*, vol. 25, no. 1, pp. 234–238, Jan. 2020.

[31] D. Song, W. Shin, and J. Lee, "A maximum throughput design for wireless powered communication networks with IRS-NOMA," *IEEE Wireless Commun. Lett.*, vol. 10, no. 4, pp. 849–853, Apr. 2020.

[32] Q. Wu, X. Zhou, and R. Schober, "IRS-assisted wireless powered NOMA: Do we really need different phase shifts in DL and UL?" *IEEE Commun. Lett.*, vol. 10, no. 7, pp. 1493–1497, Jul. 2021.

[33] B. Lyu, P. Ramezani, H. T. Dinh, and A. Jamalipour, "IRS-assisted downlink and uplink NOMA in wireless powered communication networks," *IEEE Trans. Veh. Technol.*, Jan. 2022.

[34] J. Choi, L. Cantos, J. Choi, and Y. H. Kim, "Sum rate optimization of IRS-aided uplink muliantenna NOMA with practical reflection," *Sensors*, vol. 22, no. 12, p. 4449, Jun. 2022.

[35] F. Zhou, C. You, and R. Zhang, "Delay-optimal scheduling for IRS-aided mobile edge computing," *IEEE Wireless Commun. Lett.*, vol. 10, no. 4, pp. 740–744, Apr. 2020.

[36] G. Li, M. Zeng, D. Mishra, L. Hao, Z. Ma, and O. A. Dobre, "Latency minimization for IRS-aided NOMA MEC systems with WPT-enabled IoT devices," *IEEE Internet Things J.*

[37] H. Sun, X. Ma, and R. Q. Hu, "Adaptive federated learning with gradient compression in uplink NOMA," *IEEE Trans. Veh. Technol.*, vol. 69, no. 12, pp. 16 325–16 329, Sep. 2020.

[38] X. Ma, H. Sun, and R. Q. Hu, "Scheduling policy and power allocation for federated learning in NOMA based MEC," in *Proc. IEEE GLOBECOM*, Taipei, Taiwan, 2020, pp. 1–7.

[39] Y. Wu, Y. Song, T. Wang, L. Qian, and T. Q. Quek, "Non-orthogonal multiple access assisted federated learning via wireless power transfer: A cost-efficient approach," *IEEE Trans. Commun.*, Feb. 2022.

[40] H. Liu, X. Yuan, and Y.-J. A. Zhang, "Reconfigurable intelligent surface enabled federated learning: A unified communication-learning design approach," *IEEE Trans. Wireless Commun.*, vol. 20, no. 11, pp. 7595–7609, Jun. 2021.

[41] W. Ni, Y. Liu, Z. Yang, H. Tian, and X. Shen, "Federated learning in multi-RIS aided systems," *IEEE Internet Things J.*, 2021.

[42] Z. Wang, J. Qiu, Y. Zhou, Y. Shi, L. Fu, W. Chen, and K. B. Letaief, "Federated learning via intelligent reflecting surface," *IEEE Trans. Wireless Commun*, vol. 21, no. 2, pp. 808–822, Jul. 2021.

[43] W. Ni, Y. Liu, Y. C. Eldar, Z. Yang, and H. Tian, "STAR-RIS integrated nonorthogonal multiple access and over-the-air federated learning: Framework, analysis, and optimization," *IEEE Internet Things J.*, vol. 9, no. 18, pp. 17 136–17 156, Sep. 2022.

[44] W. Ni, Y. Liu, Z. Yang, H. Tian, and X. Shen, "Integrating over-the-air federated learning and non-orthogonal multiple access: What role can RIS play?" *IEEE Trans. Wireless Commun.*, vol. 21, no. 12, pp. 10 083–10 099, Dec. 2022.

[45] J. Zheng, H. Tian, W. Ni, W. Ni, and P. Zhang, "Balancing accuracy and integrity for reconfigurable intelligent surface-aided over-the-air federated learning," *IEEE Trans. Wireless Commun.*, vol. 21, no. 12, pp. 10 964–10 980, Dec. 2022.

[46] K. Zhu and E. Hossain, "Virtualization of 5G cellular networks as a hierarchical combinatorial auction," *IEEE Trans. Mobile Comput.*, vol. 15, no. 10, pp. 2640–2654, Dec. 2015.

[47] M. H. Hajiesmaili, L. Deng, M. Chen, and Z. Li, "Incentivizing device-to-device load balancing for cellular networks: An online auction design," *IEEE J. Sel. Areas Commun.*, vol. 35, no. 2, pp. 265–279, Feb. 2017.

[48] T. H. T. Le, N. H. Tran, T. LeAnh, T. Z. Oo, K. Kim, S. Ren, and C. S. Hong, "Auction mechanism for dynamic bandwidth allocation in multi-tenant edge computing," *IEEE Trans. Veh. Technol.*, vol. 69, no. 12, pp. 15 162–15 176, Nov. 2020.

[49] Z. Zhao, C. Feng, W. Hong, J. Jiang, C. Jia, T. Q. Quek, and M. Peng, "Federated learning with non-iid data in wireless networks," *IEEE Trans. Wireless Commun.*, vol. 21, no. 3, pp. 1927–1942, Sep. 2021.

[50] B. R. Marks and G. P. Wright, "A general inner approximation algorithm for nonconvex mathematical programs," *Operations research*, vol. 26, no. 4, pp. 681–683, Aug. 1978.

[51] S. Zhang and Y. Huang, "Complex quadratic optimization and semidefinite programming," *SIAM Journal on Optimization*, vol. 16, no. 3, pp. 871–890, 2006.

[52] N. C. Luong, N. T. T. Van, S. Feng, H. T. Nguyen, D. Niyato, and D. I. Kim, "Dynamic network service selection in IRS-assisted wireless networks: A game theory approach," *IEEE Trans. Veh. Technol.*, vol. 70, no. 5, pp. 5160–5165, May 2021.

[53] Y. Gao, C. Yong, Z. Xiong, D. Niyato, Y. Xiao, and J. Zhao, "A stackelberg game approach to resource allocation for IRS-aided communications," in *Proc. IEEE GLOBECOM*, Taipei, Taiwan, 2020, pp. 1–6.

[54] S. Wang, T. Tuor, T. Salonidis, K. K. Leung, C. Makaya, T. He, and K. Chan, "Adaptive federated learning in resource constrained edge computing systems," *IEEE J. Sel. Areas Commun.*, vol. 37, no. 6, pp. 1205–1221, Mar. 2019.

[55] W. Shi, S. Zhou, Z. Niu, M. Jiang, and L. Geng, "Joint device scheduling and resource allocation for latency constrained wireless federated learning," *IEEE Trans. Wireless Commun.*, vol. 20, no. 1, pp. 453–467, Sep. 2020.

[56] Y. Zhao, M. Li, L. Lai, N. Suda, D. Civin, and V. Chandra, "Federated learning with non-iid data," *arXiv preprint arXiv:1806.00582*, 2018.

[57] M. Grant and S. Boyd, "CVX: Matlab software for disciplined convex programming, version 2.1," http://cvxr.com/cvx, Mar. 2014.

[58] W. Ni, X. Liu, Y. Liu, H. Tian, and Y. Chen, "Resource allocation for multi-cell IRS-aided NOMA networks," *IEEE Trans. Wireless Commun.*, vol. 20, pp. 4253–4268, Feb. 2021.

[59] M. Chen, S. C. Liew, Z. Shao, and C. Kai, "Markov approximation for combinatorial network optimization," *IEEE Trans Inf. Theory*, vol. 59, no. 10, pp. 6301–6327, Oct. 2013.

[60] J. Wang, D. Yang, J. Tang, and M. C. Gursoy, "Enabling radio-as-a-service with truthful auction mechanisms," *IEEE Trans. Wireless Commun.*, vol. 16, no. 4, pp. 2340–2349, Apr. 2017.

[61] Y. LeCun, L. Bottou, Y. Bengio, and P. Haffner, "Gradient-based learning applied to document recognition," *Proc. of the IEEE*, vol. 86, no. 11, pp. 2278–2324, Nov. 1998.

[62] H. H. Yang, Z. Liu, T. Q. Quek, and H. V. Poor, "Scheduling policies for federated learning in wireless networks," *IEEE Trans. Commun.*, vol. 68, no. 1, pp. 317–333, Sep. 2019.

Tra Huong Thi Le received the B.S. and M.S. degrees in electric and electronics engineering from the Ho Chi Minh City University of Technology, Ho Chi Minh City, Vietnam, in 2010 and 2012, respectively. In 2021, she received the Ph.D. degree in Computer Science and Engineering, Kyung Hee University (KHU). She was with the department of Electronics and Information Convergence Engineering, KHU from 2021 to 2022 as a postdoctoral researcher. Her research interests include resource management, game theory and machine learning.

Luggi Cantos received the B.S. degree in electronics and telecommunications engineering from Escuela Superior Politécnica del Litoral, Ecuador, in 2013 and M.S. degree in Electronic Engineering from Kyung Hee University (KHU) in 2020. He is currently pursuing his Ph.D. degree in the department of Electronics and Information Convergence Engineering, KHU. His research interests include massive MIMO, intelligent reflecting surface, and wireless powered communication.

Shashi Raj Pandey (M'21) is currently working as a Postdoctoral Researcher at the Connectivity Section, Aalborg University, Denmark. He received his B.E. degree in Electrical and Electronics with a specialization in Communication from Kathmandu University, Nepal, and the Ph.D. degree in Computer Science and Engineering from Kyung Hee University, South Korea. He served as a Network Engineer at Huawei Technologies Nepal Co. Pvt. Ltd, Nepal from 2013 to 2016. His research interests include network economics, game theory, wireless communications, data markets and distributed machine learning. He was a Member at Large at the IEEE Communication Society Young Professionals 2020 – 2021. He currently serves as a Member at Large in the IEEE Communication Society On-Line Content Board and is in the editorial advisory board of IEEE's The Institute 2022 – 2024.

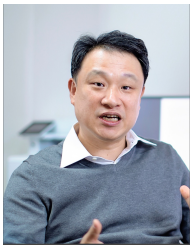

Hyundong Shin (Fellow, IEEE) received the B.S. degree in Electronics Engineering from Kyung Hee University (KHU), Yongin-si, Korea, in 1999, and the M.S. and Ph.D. degrees in Electrical Engineering from Seoul National University, Seoul, Korea, in 2001 and 2004, respectively. During his postdoctoral research at the Massachusetts Institute of Technology (MIT) from 2004 to 2006, he was with the Laboratory for Information Decision Systems (LIDS). In 2006, he joined the KHU, where he is currently a Professor in the Department of Electronic Engineering. His research interests include quantum information science, wireless communication, and machine intelligence. Dr. Shin received the IEEE Communications Society's Guglielmo Marconi Prize Paper Award (2008) and William R. Bennett Prize Paper Award (2012). He served as the Publicity Co-Chair for the IEEE PIMRC (2018) and the Technical Program Co-Chair for the IEEE WCNC (PHY Track 2009) and the IEEE GLOBECOM (Communication Theory Symposium 2012 and Cognitive Radio and Networks Symposium 2016). He was an Editor of IEEE TRANSACTIONS ON WIRELESS COMMUNICATIONS (2007–2012) and IEEE COMMUNICATIONS LETTERS (2013–2015).

Yun Hee Kim (S'97-M'00-SM'05) received the B.S.E. (*summa cum laude*), M.S.E., and Ph.D. degrees from Korea Advanced Institute of Science and Technology, Daejeon, Korea, in 1995, 1997, and 2000, respectively, all in electrical engineering. She was with the Electronics and Telecommunications Research Institute, Daejeon, Korea, as a senior research staff from 2000 to 2004. In 2004, she joined Kyung Hee University, Yongin, Korea, where she is currently a Professor in the department of Electronic Engineering. In 2000 and 2011, she was with University of California at San Diego, La Jolla, CA, USA, as a Visiting Researcher. Her research interests include wireless communication, signal processing, and artificial intelligence. She currently serves as an Editor of JOURNAL OF COMMUNICATIONS AND NETWORKS and ICT EXPRESS.